



The mean state and variability of the North Atlantic circulation: a perspective from ocean reanalyses

L C Jackson¹, C Dubois^{2,3}, G Forget⁴, K Haines⁵, M Harrison⁶, D Iovino⁷, A Köhl⁸, D Mignac⁹, S Masina⁷, K A Peterson^{1,10}, C G Piecuch¹¹, C Roberts¹², J Robson¹³, A Storto^{7,14}, T Toyoda¹⁵, M Valdivieso⁹, C Wilson¹⁶, Y Wang¹⁷,
H Zuo¹²

¹Met Office Hadley Centre, UK

²Mercator Ocean International, France

³Météo France, France

⁴MIT, USA

⁵Department of Meteorology and National Centre for Earth Observation, University of Reading, UK

⁶GFDL, USA

⁷Foundation Euro-Mediterranean Centre on Climate Change, Italy

⁸Institute of Oceanography, University of Hamburg, Germany

⁹Department of Meteorology, University of Reading, UK

¹⁰Environmental Numerical Research Section, Environment and Climate Change Canada, Canada

¹¹Woods Hole Oceanographic Institution, USA

¹²The European Centre for Medium-Range Weather Forecasts, UK

¹³National Centre for Atmospheric Science, Department of Meteorology, University of Reading, UK

¹⁴NATO STO Centre for Maritime Research and Experimentation, Italy

¹⁵Meteorological Research Institute, Japan Meteorological Agency, Japan

¹⁶National Oceanography Centre, Liverpool, UK

¹⁷Nansen Environmental and Remote Sensing Centre/Bjerknes Center for Climate Research, Norway

Key Points:

- Ocean reanalyses are potentially useful tools for understanding ocean circulation.
- Some consistency among reanalyses in interannual and decadal variability of the circulation.
- Improvements in some aspects of the ocean circulation as the observational coverage has improved.

Corresponding author: Laura Jackson, laura.jackson@metoffice.gov.uk

This article has been accepted for publication and undergone full peer review but has not been through the copyediting, typesetting, pagination and proofreading process which may lead to differences between this version and the Version of Record. Please cite this article as doi: 10.1029/2019JC015210

Abstract

The observational network around the North Atlantic has improved significantly over the last few decades with subsurface profiling floats and satellite observations, and the recent efforts to monitor the Atlantic Meridional Overturning Circulation (AMOC). These have shown decadal timescale changes across the North Atlantic including in heat content, heat transport and the circulation. However there are still significant gaps in the observational coverage. Ocean reanalyses integrate the observations with a dynamically consistent ocean model and can be used to understand the observed changes. However the ability of the reanalyses to represent the dynamics must also be assessed.

We use an ensemble of global ocean reanalyses to examine the time mean state and interannual-decadal variability of the North Atlantic ocean since 1993. We assess how well the reanalyses are able to capture processes and whether any understanding can be gained. In particular we examine aspects of the circulation including convection, AMOC and gyre strengths, and transports. We find that reanalyses show some consistency, in particular showing a weakening of the subpolar gyre and AMOC at 50°N from the mid-90s until at least 2009 (related to decadal variability in previous studies), a strengthening and then weakening of the AMOC at 26.5°N since 2000, and impacts of circulation changes on transports. These results agree with model studies and the AMOC observations at 26.5°N since 2005. We also see less spread across the ensemble in AMOC strength and mixed layer depth, suggesting improvements as the observational coverage has improved.

Plain language summary

The observational network around the North Atlantic has improved significantly over the last few decades revealing changes over decadal timescales in the North Atlantic, including in heat content, heat transport and the circulation. However there are still significant gaps in the observational coverage. Ocean reanalyses fill in these gaps by combining the observations with a computer model of the ocean to give consistent estimates of the ocean state. These reanalyses are potentially useful tools that can be used to understand the observed changes, however their skill must also be assessed.

We use an ensemble of global ocean reanalyses in order to examine the mean state and variability of the North Atlantic ocean since 1993. In particular we examine the con-

61 vection, the circulation, transports of heat and fresh water and temperature and salin-
62 ity changes. We find that reanalyses show some consistency in their results, suggesting
63 that they may be useful for understanding circulation changes in regions and times where
64 there are no observations. We also show improvements in some aspects of the ocean cir-
65 culation as the observational coverage has improved. This highlights the importance of
66 continuing observational campaigns.

67 **1 Introduction**

68 Although the North Atlantic has warmed since preindustrial times (Collins et al.,
69 2013), it has also exhibited large variability on different timescales, particularly of up-
70 per ocean temperatures (Knight, Allan, Folland, Vellinga, & Mann, 2005; Sutton et al.,
71 2018). This variability has been shown to have wide-ranging impacts, for instance on pre-
72 cipitation in Europe (Sutton & Dong, 2012), the North Atlantic storm track (Peings &
73 Magnusdottir, 2014), monsoons, and hurricane frequency (Smith et al., 2010; R. Zhang
74 & Delworth, 2006). As well as decadal and multi-decadal variability, there has also been
75 significant interannual variability, such as significant cooling of the subtropics in 2010
76 and the recent cooling of the subpolar gyre (Cunningham et al., 2013; Grist et al., 2016).
77 These sea surface temperature anomalies can influence the weather and climate over Eu-
78 rope (Josey et al., 2018), in particular through influencing the winter North Atlantic Os-
79 cillation (Cassou, Deser, & Alexander, 2007), summer precipitation (Dunstone et al., 2018)
80 and potentially heat waves (Duchez et al., 2016). Increasing observational coverage over
81 the last few decades, particularly with satellite measurements of sea level and sea sur-
82 face temperatures (SST), and the Argo network providing temperature and salinity pro-
83 files, has revealed large changes in ocean properties and generated a need to understand
84 the processes driving the changes (Robson, Sutton, Archibald, & et al., 2018; von Schuck-
85 mann & et al, 2018).

86 In the subpolar gyre a warming was observed in the late 1990s, and several model-
87 based studies have now attributed this warming to increased northwards heat transport
88 due to a strong Atlantic Meridional Overturning Circulation (AMOC) (Robson, Sutton,
89 Lohmann, Smith, & Palmer, 2012; Williams, Roussenov, Smith, & Lozier, 2014; Yeager
90 & Danabasoglu, 2014), while some reanalysis studies (Piecuch, Ponte, Little, Buckley,
91 & Fukumori, 2017; Yang, Masina, Bellucci, & Storto, 2016) suggest that changes in gyre
92 advection were important as well. Although we do not have direct measurements of the

93 strength of the AMOC during this period, model experiments generally agree that the
94 AMOC in the subpolar region was strong in the mid 90s and weakened over the follow-
95 ing decade (Danabasoglu et al., 2016; Robson et al., 2012). Similarly the subpolar gyre
96 (SPG) strength was found to be strong in the mid 90s and then weakened, in agreement
97 with proxies for SPG strength based on altimeter data (Häkkinen & Rhines, 2004). Stud-
98 ies have linked the strong AMOC and SPG circulations in the mid 1990s to increased
99 densities in the Labrador Seas caused by buoyancy forcing during a persistently posi-
100 tive phase of the North Atlantic Oscillation (NAO) in the preceding years (Deshayes &
101 Frankignoul, 2008; Eden & Willebrand, 2001; Lohmann, Drange, & Bentsen, 2009; Rob-
102 son et al., 2012; Yang et al., 2016; Yeager & Danabasoglu, 2014). However recent obser-
103 vations have suggested that the AMOC could be more influenced by water mass trans-
104 formations to the east of Greenland (Lozier et al., 2019). More recently the warming and
105 salinification of the subpolar region has reversed to a cooling and freshening, consistent
106 with weakening heat and salt transports (Hermanson et al., 2014; Robson, Ortega, & Sut-
107 ton, 2016), although there is also strong evidence that the more extreme cooling seen in
108 2014 was caused by anomalous surface heat fluxes (Grist et al., 2016; Josey et al., 2018).
109 This cooling has resulted in an increase in density in the Labrador Seas, with an asso-
110 ciated increase in deep convection (Yashayaev & Loder, 2017).

111 In the subtropics the variability has been markedly different with interannual vari-
112 ability superimposed on a more gradual warming trend (Robson et al., 2018; Williams
113 et al., 2014). The AMOC at 26.5°N has been monitored since 2004 by the RAPID-MOCHA
114 array (McCarthy et al., 2015) revealing interannual variability including a large, tem-
115 porary weakening in winter 2009-2010, believed to be wind-driven (Evans et al., 2017;
116 McCarthy et al., 2012; C. D. Roberts et al., 2013a) that caused a cooling of the subprop-
117 tics (Cunningham et al., 2013). The AMOC strength has also weakened since 2004, and
118 has been found to be in a weaker state since 2008 (Smeed et al., 2018). Although there
119 have been suggestions of a longer term (centennial) weakening (Caesar, Rahmstorf, Robin-
120 son, Feulner, & Saba, 2018; Thornalley et al., 2018), there is some evidence that the ob-
121 served decadal weakening is due to decadal variability (Jackson, Peterson, Roberts, &
122 Wood, 2016). Prior to 2004 there were only intermittent measurements of AMOC strength.
123 Although modeling studies mostly agree that the AMOC in the subpolar gyre was strong
124 in the mid 90s and then weakened, there is more disagreement amongst models about
125 the changes in the subtropical gyre (Danabasoglu et al., 2016). Jackson et al. (2016), us-

126 ing an ocean reanalysis that agreed well with the RAPID observations, suggested that
127 the AMOC at 26.5°N increased over the decade up to 2004 and then weakened after as
128 a lagged response to the weakening of the subpolar AMOC and Labrador Sea densities
129 during the previous decade. Previous model-based studies have also shown a lagged re-
130 lationship between the subpolar and subtropical AMOC (Yeager & Danabasoglu, 2014),
131 and a relationship of the AMOC with densities in the Labrador Sea (Robson, Hodson,
132 Hawkins, & Sutton, 2014).

133 A greater understanding of these processes can help to separate natural variabil-
134 ity from anthropogenic change. It is also fundamental to our ability to make predictions
135 on interannual to centennial timescales. However observations are still limited, partic-
136 ularly when it comes to transports and process-related quantities such as convection. Ocean
137 and climate models are useful tools in studying such processes, however they suffer from
138 biases and can show a wide range of timescales and driving processes of variability. One
139 tool that has been less used so far is the ocean reanalysis. Reanalyses are ocean mod-
140 els that are forced by meteorological boundary conditions from atmospheric reanalyses
141 and assimilate observations such as in situ temperature and salinity, SST, sea level anoma-
142 lies and sea ice concentration (Storto et al., 2019). As such, they integrate the observa-
143 tions within a dynamically consistent ocean model, although the assimilation itself can
144 alter the dynamics. Reanalyses differ with regard to the types of observations assimi-
145 lated, the method of assimilation, the surface forcing, and of course the ocean model used
146 (Balmaseda et al., 2015), with those designed to cover the satellite period able to use more
147 observational types than those covering longer periods. An advantage of reanalyses as
148 compared to other data products is that they can provide transports, and other prop-
149 erties, that can be hard to measure continuously. However care must be taken that the
150 reanalysis is sufficiently constrained by the observations in the region of interest, and that
151 the constraints themselves do not adversely affect the processes involved creating spu-
152 rious results (Storto et al., 2019). Multimodel ensembles can help interpretation by pro-
153 viding a range of possible behaviors (Masina et al., 2017; Storto et al., 2018). There is
154 also temporal variability in the type and number of observations assimilated, so users
155 must be aware that the quality of the reanalysis for a particular purpose could change
156 in time.

157 The ORA (Ocean Reanalysis) Intercomparison Project was initiated under CLI-
158 VAR GSOP and GODAE-Oceanview and has produced a series of papers examining global

159 ocean reanalyses and focusing on different aspects of the ocean state (e.g. steric sea level,
160 air-sea fluxes, ocean heat and salt content among others). These were then brought to-
161 gether in a special issue of *Climate Dynamics* (Balmaseda et al., 2015; Chevallier et al.,
162 2017; Karspeck et al., 2017; Masina et al., 2017; Palmer et al., 2017; Shi et al., 2017; Storto
163 et al., 2017; Tietsche, Balmaseda, Zuo, & Mogensen, 2017; Toyoda et al., 2017a, 2017b;
164 Valdivieso et al., 2017). A further paper on the polar oceans was later added (Uotila et
165 al., 2018). Most of these papers focused on consistency of the mean states amongst re-
166 analyses although several also looked at diagnostics of variability. Palmer et al. (2017)
167 showed many reanalyses had consistent ocean heat content (OHC) trends as a function
168 of depth, and that a significant component of recent OHC increase was below 700m depth.
169 The North Atlantic was seen to be an area of substantial agreement in upper OHC trends,
170 consistent with this being a better observed region. However there have been substan-
171 tial disagreements shown across reanalyses: Karspeck et al. (2017) looked at the AMOC
172 in long reanalyses starting before 1960, and found disagreement in AMOC variability and
173 strength in these early, observation-sparse periods.

174 This study advances beyond many previous ORA studies in presenting a more pro-
175 cess oriented approach aimed at understanding differences and similarities. We focus on
176 the dynamics of the North Atlantic since 1993, which is when satellite altimetry data
177 (e.g. see Forget and Ponte (2015)) became routinely available and vastly increased the
178 observations that could be assimilated in a reanalysis. Over this period the increase in
179 observations has also revealed changes in temperature and salinity in the North Atlantic,
180 along with changes in circulation patterns both observed and inferred. The aim of this
181 study is to examine the climatology and inter-annual to decadal changes of the North
182 Atlantic ocean in a multi-model ensemble of global ocean reanalyses. In particular we
183 ask: Where is there agreement or disagreement across reanalyses? Can we learn what
184 makes reanalyses good at specific processes? Can these reanalyses improve our under-
185 standing of the dynamics in the North Atlantic ocean?

186 Section 2 describes the reanalyses used. We then discuss the climatologies of the
187 products in section 3 and the changes seen in section 4. Section 5 provides a discussion
188 and summary. We also list acronyms used in Table 1.

2 Models and methods

2.1 Reanalyses

In this study, we have analyzed data from eleven ORA products (C-GLORSv7, ECCO V4 R3, ECDA3, GECCO2, GLORYS2v4, GLORYS12v1, GloSea5, GONDOLA100A, NorCPM-v1, ORAS5 and UR025.4) in the North Atlantic (Table 2). It should also be noted that 6 of the reanalyses use the NEMO ocean model and 5 of these use the same resolution (0.25°). The latest addition to this set of NEMO reanalyses is the higher resolution ($1/12^\circ$) GLORYS12v1 reanalysis that has been included in this study. Although these reanalyses use very similar models and assimilated data, they do differ in the assimilation techniques used, and there are still many interesting differences in the results (Storto et al., 2018). The other products however cover a wide range of model systems, resolutions, and data assimilation approaches. ECCO V4 R3 and GECCO2 use a 4DVar assimilation scheme which optimizes the solution through adjusting parameters (including surface fluxes, wind stresses, mixing parameters) rather than apply increments in temperature and salinity. The NorCPM-v1 reanalysis has a coupled atmospheric component and hence has quite different surface fluxes and wind stresses from the other reanalyses, which are forced by atmospheric reanalysis fields. In NorCPM-v1 there is no atmospheric constraint and assimilation is only carried on the ocean component (weakly coupled data assimilation). The adjustment in the other components (atmosphere, sea ice) occurs dynamically during the integration of the system. NorCPM-v1 is also an outlier in being the only reanalysis using anomaly rather than full field assimilation, hence its mean state is unconstrained by observations. We do include it in the analysis for completeness.

2.2 Observational data

Where appropriate we also compare the ensemble to observational estimates, although in some circumstances suitable observational estimates are not available. We include temperatures, salinities and densities from the gridded observational analyses EN4 (Good, Martin, & Rayner, 2013) and CORA (Cabanes et al., 2013). These use some of the same data as assimilated in the reanalyses (in particular subsurface temperature and salinity profiles), however they use statistical techniques to infill missing data, rather than assimilation in a dynamical model. We also include AMOC volume and heat transports from the RAPID-MOCHA array (Johns et al., 2011; McCarthy et al., 2015; Smeed et

220 al., 2017), volume transports from the new OSNAP array (Lozier et al., 2019) and var-
221 ious estimates of the meridional heat and freshwater transports from sections across the
222 North Atlantic. We also include a comparison with the climatological estimate of the March
223 mixed layer depth from de Boyer-Montegut, Madec, Fischer, Lazar, and Iudicone (2004).

224 **2.3 Methods**

225 Definitions of individual diagnostics are included in the sections and figure captions.
226 Not all data were made available from all reanalyses, hence not all reanalyses are included
227 in all figures.

228 We use climatologies based on the years 1993-2010 since that is the common pe-
229 riod available for all reanalyses, apart from mixed layer depths where we use a more re-
230 cent period (2004-2010) since there is large uncertainty earlier than that. Timeseries are
231 shown for the full period (since 1993) for each reanalysis, some of which extend to 2017.
232 For timeseries we use monthly means where available (some diagnostics were only avail-
233 able as annual means for NorCPM-v1). We examine interannual to decadal changes by
234 smoothing monthly values with a 12 month running mean, which also has the advantage
235 of removing the seasonal cycle. Timeseries are shown as either the total value (with smooth-
236 ing) or as anomalies from the climatology of the relevant reanalysis.

237 Significance of relationships between two variables are tested using a null hypoth-
238 esis that there is no correlation or no trend and a 95% confidence interval ($p=0.05$). Cor-
239 relation coefficients (R) and probabilities of the null test (p) are quoted. In particular
240 the correlations of scatter plots between two variables or between two timeseries are tested
241 using a t test (with the null hypothesis that there is no correlation). Significance of a
242 trend in a timeseries is tested against the variability of that timeseries (using a t test and
243 the null hypothesis that the trend is zero). The significance of a difference between two
244 n -year means is tested in comparison with the bootstrapped distribution of differences
245 between n -year means.

246 **3 Mean state**

247 **3.1 Convection and formation of deep water masses**

248 March mixed layer depth climatologies are shown in Fig 1 (see caption for defini-
249 tion). These are often used as a proxy for deep convection, which alters densities in the

250 subpolar North Atlantic and hence affects ocean dynamics. There are two centres of deep
251 convection in observations and reanalyses: in the Labrador and GIN (Greenland-Iceland-
252 Norway) Seas. About half the reanalyses have depths of convection in the Labrador Seas
253 that are comparable to the observational climatology (although this is based on a much
254 longer time period, (de Boyer-Montegut et al., 2004)). The other half have too deep and
255 widespread convection, apart from GECCO2 where the mixed layer depth is very shal-
256 low. Most reanalyses have much too deep convection in the GIN seas, as has been noted
257 in a previous reanalysis comparison (Uotila et al., 2018) and seen in coupled climate mod-
258 els (Heuzé, 2017). A previous comparison of mixed layer depths across reanalyses was
259 also made by Toyoda et al. (2017a) who looked globally at shallow mixed layer depths,
260 rather than regions of deep convection. They do note that there is little consistency amongst
261 and between observational and reanalyses data sets at high latitudes.

262 3.2 Circulation

263 The AMOC streamfunction in many reanalyses looks similar to that found in free-
264 running models (Danabasoglu et al., 2014), with a North Atlantic overturning cell in the
265 upper 3000m (Fig 2). This depicts the northwards volume transport in the upper 1000m
266 of the Atlantic, followed by sinking and a southwards return flow between 1000-3000m
267 approximately. In common with free-running models there are considerable differences
268 in the latitude of the streamfunction maximum (Danabasoglu et al., 2016). In some cases
269 there are discontinuities at some latitudes, possibly suggesting an impact of the assim-
270 ilation scheme. In particular, GloSea5 is suspect in the South Atlantic and near the equa-
271 tor (where there is a discontinuity in streamfunction strength): this issue has been traced
272 to the method of assimilating sea surface height, and will be the subject of a future pub-
273 lication (M. Bell, personal communication). In most reanalyses the reversed Antarctic
274 Bottom Water cell below 3000m is very weak compared to forced and coupled models
275 (Ba et al., 2014; Danabasoglu et al., 2016). This could be because there is little constraint
276 from data at these depths.

277 One place where the AMOC has been continuously monitored is at 26.5°N, where
278 the RAPID array (McCarthy et al., 2015) has been in place since 2004. Reanalysis pro-
279 files of the AMOC at this section (Fig 2, are calculated here using the same methodol-
280 ogy as the observations (see C. D. Roberts et al. (2013a)) and for the same time period
281 (2004-2010)). They show upper northwards transport (increasing streamfunction with

282 depth) and deeper southwards transport (decreasing streamfunction). There is mostly
283 a good agreement with the observations for the value and depth of the streamfunction
284 maximum, although some reanalyses have too shallow a return flow. Previous studies
285 have noted that data assimilation usually improves the AMOC mean strength over that
286 in forced ocean only models (Balmaseda et al., 2007; Karspeck et al., 2017; Tett, Sher-
287 win, Shrivastava, & Browne, 2014).

288 Recently observations of the AMOC in the subpolar gyre have begun with the OS-
289 NAP initiative (Lozier et al., 2017). These have calculated an AMOC in density space
290 with time mean profiles (Fig 13a) showing a northwards transport of Atlantic waters be-
291 tween densities 1027.2-1027.6 kg/m³ and a denser return flow. There is also a small south-
292 wards transport of very light, surface waters. There is a good agreement with the mag-
293 nitudes of the AMOC (14.9 ± 0.9 Sv) and the density at which the profile peaks in the
294 observations (Lozier et al., 2019). Some reanalyses have a stronger overturning, however
295 we note that the observational time series is short so far (<2 years), so the observational
296 error on the long term mean is uncertain.

297 To assess the large-scale horizontal circulation we can compare the vertically in-
298 tegrated (barotropic) streamfunctions (Fig 3). These are the vertically integrated stream-
299 functions and are referenced to values on the eastern Atlantic coasts. They show two gyres:
300 an anticyclonic subtropical gyre (STG) and cyclonic subpolar gyre (SPG), depicting the
301 vertically integrated velocities. The medium (0.25°) and high (1/12°) resolution reanal-
302 yses clearly show more fine-scale features and a very localized intensification of the Gulf
303 Stream near the western boundary, whereas lower resolution reanalyses have smoother
304 subtropical gyres with generally broader boundary currents. This may be because of a
305 greater influence of inertial recirculations at higher resolution, as previously found by
306 Yeager (2015). Treguier, Deshayes, Lique, Dussin, and Molines (2012) also found that
307 increased resolution strengthened the Gulf Stream.

308 To directly compare the circulations we split the STG and SPG into 4 boxes (Fig
309 4) covering the western boundary and interior regions. There is consistency between the
310 interior gyre strength in the 6 NEMO models, and with ECCO V4 R3 and ECDA3. The
311 outliers are NorCPM-v1 (which does not constrain the mean state) and GECCO2 where
312 the interior STG is stronger than other reanalyses (see also subtropical gyre in Fig. 3).
313 ECCO V4 R3 and GECCO2 use 4DVar which modifies surface fluxes within given er-

314 ror bounds, including wind stresses that have a strong impact on the gyre strengths through
315 Sverdrup dynamics. Hence it is likely that modifications to wind stresses in GECCO2
316 have changed the gyre strengths, though we note that ECCO V4 R3 (which uses differ-
317 ent wind forcing products as the initial estimate and different optimization windows and
318 iterations) has gyre strengths more consistent with other reanalyses.

319 In the interior of the subtropics the NorCPM-v1 and GONDOLA100A upper layer
320 gyres are weaker (with smaller interior southward flow) but their gyres are deeper with
321 perhaps 30% of the flow below 1100m, while most products have weaker deep interior
322 southward flows. GECCO2 has a strong deep flow as well as a strong upper layer flow.
323 We see no relationship between the depth of the interior flow and the depth of the AMOC
324 circulation (Fig 2).

325 A comparison of the time mean strength of various circulation metrics is shown in
326 Fig 5. There is a marginally significant relationship with reanalyses that have denser up-
327 per Labrador Sea (LS) densities having a stronger AMOC at 50°N ($R = 0.60$, $p = 0.06$,
328 Fig 5a). This is in agreement with results from an ocean only model intercomparison (Dan-
329 abasoglu et al., 2014). Observational products (EN4 and CORA) show large uncertain-
330 ties in the densities of the upper LS, however they suggest that those NEMO reanaly-
331 ses with lighter upper LS and weaker AMOC at 50°N (M50) are less realistic. There is
332 no significant correlation between the AMOC at 26.5°N (M26) and either M50 or the
333 deeper Labrador Sea density (Fig 5b,c). Reanalyses with a stronger (more negative) SPG
334 tend to have a weaker subpolar AMOC. This relationship is not significant ($R = 0.58$,
335 $p = 0.13$, Fig 5d), though we note that the sample size is small. Danabasoglu et al. (2014)
336 show a relationship between the AMOC strength and the Labrador Sea mixed layer depth
337 (MLD), however we do not see such a relationship, possibly because the MLD is very
338 noisy during the first part of the timeseries in many reanalyses (Fig 9c).

339 3.3 Transports

340 Time mean meridional ocean heat and freshwater transports (OHT/OFWT) are
341 shown in Fig 6. These are calculated from monthly velocity, temperature and salinity
342 fields and so do not include fluxes from variability at a higher frequency than monthly.
343 Parameterized transports (Gent & McWilliams, 1990) are included for those reanalyses
344 that use them. The OHT is northwards at every latitude through the Atlantic, with the

345 maximum between 25 and 35 °N in most reanalyses. The OFWT has a minimum around
346 35-45°N, showing a maximum in southwards freshwater transport. A reduction (increase)
347 in OFWT as latitude increase would be balanced in steady state by an export (import)
348 of freshwater from surface fluxes.

349 Northwards heat transports (Fig 6a) at most latitudes are strongest in NorCPM-
350 v1 (maximum 1.4 PW). It does not constrain the mean state and it is likely the trans-
351 port is strong because of the strong AMOC (Fig 2). ECCO V4 R3 has the weakest heat
352 transport at most latitudes with a maximum of 0.92 PW. Other reanalyses underesti-
353 mate the transport around 26.5 °N, but mostly agree with the observational estimates
354 further north of 35°N. However it is possible that the methodology for the observational
355 estimates at 26.5°N could overestimate the heat transport (Stepanov, Iovino, Masina,
356 Storto, & Cipollone, 2016). GloSea5 shows a rapid drop off of the heat transport in the
357 South Atlantic caused by the very weak AMOC found there (Fig 2).

358 At 26.5°N there is a significant correlation ($R=0.79$, $p=0.02$) of the mean AMOC
359 strength with the total heat transport (Fig 7b), as seen across an ocean model ensem-
360 ble (Danabasoglu et al., 2014). The heat and freshwater transport can also be decom-
361 posed into overturning and horizontal circulation components (and throughflow compo-
362 nent for freshwater), see Bryden and Imawaki (2001); McDonagh et al. (2015). The re-
363 lationship with the total heat content occurs because of a strong correlation of the AMOC
364 with the overturning heat transport at 26.5°N ($R=0.81$, $p=0.01$, Fig 7a). However us-
365 ing this relationship to predict observed heat transports from AMOC strength, under-
366 estimates the observed heat transport (Johns et al., 2011), even when comparing with
367 the reanalyses available over the RAPID climatology period (2005-2015). This discrep-
368 ancy has been seen in many models previously (Danabasoglu et al., 2014) and in pre-
369 vious reanalyses (Masina et al., 2017). Msadek et al. (2013) attribute this to an under-
370 estimation of the gyre component (due to poor representation of the transports near the
371 western boundary) and an underestimation of the overturning part because of an overly
372 diffusive thermocline. Figure 16 shows that most reanalyses underestimate both of these
373 components.

374 Further north (50°N), the AMOC still determines the overturning part of the heat
375 transport, however the gyre transport is important as well (Fig 17). It should be noted
376 that the decomposition into gyre and overturning components in the subpolar North At-

377 lantic is less meaningful than in the subtropics since the thermohaline circulation projects
378 onto both components. We can look at the relationships with the total heat transport,
379 but find no significant relationship between the total heat transport and either the SPG
380 or M50 strength (Fig 7f,h).

381 For freshwater transport (Fig 6b), all reanalyses transport freshwater southwards
382 across the equator due to the horizontal circulation, (see (Mignac, Ferreira, & Haines,
383 2019)), other than NorCPM-v1 which is fully coupled and the atmospheric bias is a main
384 contributor to the ocean bias in the tropical Atlantic (Lübbecke et al., 2018). The NEMO
385 reanalyses all show relatively strong southward transport at 36, 45 and 53°N. They also
386 show greater transports of heat than the other reanalyses between 30 and 55°N, and this
387 may be because of their eddy-permitting resolution since ocean models have been shown
388 to have differences in heat and fresh water transport with resolution (M. J. Roberts et
389 al., 2016; Treguier et al., 2012). Observational estimates at 36°N show a wide range of
390 values and do not constrain the reanalyses.

391 There is a significant relationship ($R=-0.84$, $p=0.01$) between the overturning part
392 of the freshwater transport at 26.5°N and the AMOC (Fig 7c), but there are no signif-
393 icant relationships between the total freshwater transport and AMOC at 26.5°N ($R=-$
394 0.25 , $p=0.55$, Fig 7d) or for any freshwater components at 50°N (not shown). The fact
395 that relationships between the AMOC and freshwater transports are less significant than
396 for heat transports could be because there is, historically, less salinity data to assimilate
397 than temperature and so uncertainties can be expected to be bigger. It is also possible
398 that the distribution of salinity within the ocean results in a greater dominance of the
399 horizontal component.

400 **4 Variability**

401 **4.1 Heat and Fresh Water Content**

402 The temperature and salinity of the upper 500m of the North Atlantic shows co-
403 herent variability (Fig 8). The subtropics (25-45°N) show an increase towards warmer
404 and more saline conditions, although there is more agreement across reanalyses in the
405 temperature than salinity changes. This warming and salinification is consistent with
406 anthropogenically driven trends towards a warmer and saltier subtropics, likely caused
407 by anthropogenic changes in surface fluxes (Rhein et al., 2013). Monitoring volumetric

408 changes above some temperature or salinity criteria can help identify thermohaline changes
409 associated with water mass redistribution (which can change the volume of water above
410 this criteria) as opposed to air-sea exchange (which only directly change the near-surface
411 temperature or salinity) (Evans et al., 2017; Palmer & Haines, 2009). However we note
412 that assimilation could also cause volumetric changes. This volumetric analysis is shown
413 in Fig 8 using the volume of water greater than 10°C or 35.3 PSU; these criteria are cho-
414 sen to represent the subtropical pycnocline. Some reanalyses show an increase in the vol-
415 ume of warm water in the subtropics, particularly since 2000, suggesting that water mass
416 redistribution (such as advection) may also be playing a role, however this signal is not
417 consistent across reanalyses.

418 In the subpolar region (45-65°N) there is an increase in temperature and salinity
419 from the mid 90s to around 2005, and then a decrease, with the largest cooling seen in
420 2014. The volumetric analysis shows similar changes, suggesting a role for advection in
421 these decadal scale changes. This is in agreement with previous studies showing the warm-
422 ing and cooling of the subpolar gyre through changes in advection (Hermanson et al.,
423 2014; Piecuch et al., 2017; Robson et al., 2016, 2012). However we note that the large
424 cooling seen in 2014 has been attributed to surface fluxes (Grist et al., 2016; Josey et
425 al., 2018). There are other interannual signals such as the coherent subtropical cooling
426 and subpolar warming in 2010. The subtropical cooling has previously been shown to
427 have been driven by a weak AMOC and hence heat transport at 26.5°N (Cunningham
428 et al., 2013) with an important contribution driven by wind variations (Evans et al., 2017).

429 **4.2 Convection and formation of deep water masses**

430 Figure 9 shows anomalous densities in the upper (0-500m) and lower (1500-1900m)
431 Labrador Seas waters. There are significant differences between the densities of reanal-
432 yses, but most capture the general trends. Most show a decrease in 0-500 m density in
433 the late 90s and a strong increase after 2014. In the 1500-1900 m layer most reanalyses
434 show a reduction in density since the mid 90s, although the timing and magnitude of weak-
435 ening are varied. However, some reanalyses also appear to have unrealistic trends that
436 do not agree with the observations; e.g. ORAS5 has a very large initial decline in deep
437 density; GONDOLA100A has a positive density trend at depth. It should be noted, how-
438 ever, that there is less observational data in the LS, particularly in winter, prior to the
439 introduction of Argo in the early 2000s. Hence there are uncertainties in the observa-

440 tional products: an indication of the uncertainty is given by the differences in the two
441 observational products (EN4 and CORA).

442 The density of sea water is a product of the non-linear interaction between tem-
443 perature, salinity and pressure, and is complicated by the fact that temperature and salin-
444 ity effects are often largely compensated (Robson et al., 2016). Recently it has been shown
445 that systematic biases in the mean state and variability of temperature and salinity in
446 the Labrador Sea in both free-running models and reanalyses can change whether tem-
447 perature or salinity has the dominant control on density changes (Menary & Herman-
448 son, 2018; Menary, Hermanson, & Dunstone, 2016; Menary et al., 2015) . Furthermore,
449 Menary and Hermanson (2018) showed that uncertainty in this relationship has impor-
450 tant implications for initialising and evaluating near-term climate predictions. There-
451 fore, we evaluate whether temperature or salinity dominates the variability in the Labrador
452 Sea densities by computing the relative correlation between density anomalies (i.e. in-
453 cluding both changes in temperature and salinity), and the density anomalies that would
454 result from only changes in temperature or salinity. Figure 10 shows whether temper-
455 ature or salinity dominate the density variability for all the different ocean reanalyses
456 (see caption for details). In observations the density variability of surface waters (0-200m)
457 is mostly driven by salinity variability, however in deeper layers the density variability
458 is mostly driven by temperature variability. Most models agree with the observations
459 in terms of the density drivers, however there are some significant outliers. NorCPM-
460 v1 is always temperature dominated, probably because its mean state is not constrained.
461 GONDOLA100A, GECCO2 and ECCO V4 R3 also all have salinity dominated density
462 anomalies at depth, which likely explains the lack of a weakening trend in their repre-
463 sentations of densities in the 1500-1900 m layer (Fig 9b, 14b). The greater spread at depth
464 is likely because there are less observations there to constrain the ocean properties.

465 For mixed layer depth (MLD) in the Labrador Sea (Fig 9c) there is initially a large
466 spread of values with many reanalyses showing large inter-annual variability, suggest-
467 ing an inability to realistically simulate the MLD. Despite the initially large variability,
468 there is increasing consistency with time (apart from NorCPM-v1) suggesting an improve-
469 ment in representation of deep convection as observational coverage increases (around
470 the time of the introduction of Argo in the mid 2000s). Many reanalyses show a tem-
471 porary deepening in mixed layer depth in 2008 and then a sustained deepening since 2010,

472 consistent with the increase in upper ocean densities and in agreement with observations
473 of MLD (Vage et al., 2008; Yashayaev & Loder, 2017).

474 4.3 AMOC Circulation

475 Figure 11 shows the timeseries of the AMOC at 26.5 and 50°N, which are repre-
476 sentative of the variability within the subtropical and subpolar regions respectively (not
477 shown). As well as the timeseries of individual reanalyses, the figure also shows an en-
478 semble mean and spread (2 x standard deviation) of the anomalies relative to each cli-
479 matology. This allows an assessment of how much the variability agrees across the re-
480 analyses.

481 In winter 2009/10, a substantial temporary weakening of the AMOC at 26.5°N was
482 observed, linked to a strongly negative NAO. This is suggested to have been caused by
483 both Ekman (through the zonal wind stress) and wind-driven non-Ekman (through wind-
484 driven upwelling of density surfaces) components (McCarthy et al., 2012; C. D. Roberts
485 et al., 2013a). All reanalyses show a temporary weakening of the AMOC (see first col-
486 umn in Fig 11g) although this weakening is less than observed in most cases. The dips
487 captured in winters 2009/10 and 2012/13 can be partially attributed to the Ekman com-
488 ponent (blue line in Fig 11e) with many reanalyses failing to capture the non-Ekman weak-
489 ening in 2009/10 (not shown). All reanalyses show a weakening of the AMOC from 2006-
490 2013 (most of which are significant compared to the internal variability of each timeseries,
491 see methods), in agreement with the observations, although the magnitude of weaken-
492 ing is again generally smaller than in the observations (Fig 11g). All reanalyses also show
493 a brief weakening from 1999-2001 (although this is only significant in one reanalysis) and
494 then a strengthening (mostly significant) from 2001-2006.

495 Prior to 1999 the reanalyses show a larger spread in the AMOC strength at 26.5°N
496 implying greater uncertainty. The consistency of the variability across the reanalyses since
497 1999 suggests a common driving factor, and supports the results by Jackson et al. (2016)
498 that the observed AMOC decline may have been preceded by an increase. There is no
499 consistent trend over the whole period (Fig 11h), although this does not preclude a longer
500 term weakening trend. In an ensemble of forced models, Danabasoglu et al. (2016) found
501 that the AMOC at 26.5°N strengthened in the couple of decades before 1998 and then
502 showed a significant weakening from 1998-2007 in half the models. Inspection of the time-

503 series (Fig. 1 in Danabasoglu et al. (2016)), however, shows that this weakening mostly
504 occurs in the few years after 1998, with the multimodel mean showing a weakening of
505 2-3Sv between 1998-2004. This is similar to the weakening seen in our ensemble around
506 year 2000, although occurring over a longer period of time. A recent study looking at
507 the AMOC in a different ensemble of reanalyses (Karspeck et al., 2017) found little agree-
508 ment with the AMOC observed at 26.5°N, contrary to results here. We note that Kar-
509 speck et al. (2017) only considered reanalyses over the period 1960-2012 when there was
510 little data to assimilate for the majority of the period. Therefore many of the reanaly-
511 ses did not assimilate more recent sources of data such as altimeter data. This study con-
512 siders a more diverse set of reanalyses, only a few of which overlap with, or have prede-
513 cessors in, the Karspeck et al. (2017) study.

514 A more in depth comparison with the RAPID observations is made in Fig 12 which
515 shows the correlations with the observational array and standard deviations for the AMOC
516 components. Out of those reanalyses where this comparison is possible, the best corre-
517 lations with the RAPID observations are achieved with the four NEMO 0.25 reanaly-
518 ses and ECCO V4 R3. It is perhaps not surprising that there is agreement amongst the
519 NEMO reanalyses (since they use the same ocean model and observations for assimila-
520 tion), however it should be noted that they still show a range of values for the changes
521 and trends in Fig 11g,h. ECCO V4 R3 however is a very different reanalysis in that it
522 uses a different ocean model (MITgcm) and assimilation scheme. Most reanalyses also
523 underestimate the interannual variability. It should also be noted that the components
524 of the upper and lower limbs of the AMOC (apart from the Ekman component which
525 is determined by the wind fields used) compare less favorably to the observations than
526 the total (Fig 12). Although the Ekman component contributes to the agreement of the
527 total AMOC to the observations, there is also better agreement of the AMOC minus the
528 Ekman transport with observation (not shown) than any of the individual components.
529 This suggests that the resemblance to observations is through some constraint (as yet
530 unknown) of the system on the total transport, rather than through capturing individ-
531 ual components, ie resolving the Florida Straits flow and getting the depth structure of
532 the deep AMOC return flow (see also Forget (2010); Jackson et al. (2016); Kohl (2015);
533 C. D. Roberts et al. (2013a))

534 At 50°N the variability is consistent across most reanalyses although there are a
535 wide range of mean strengths (Fig 11b,d,f and Fig 2). Much of this interannual variabil-

536 ity is from the wind-driven Ekman transport (Fig 11f shows the Ekman transport cal-
537 culated from GloSea5). It is to be expected that the Ekman transport would be simi-
538 lar across the reanalyses since it is essentially prescribed through wind fields (though mod-
539 ified by ECCO V4 R3 and GECCO2). Most of the reanalyses show significant weaken-
540 ing between 1993 and 2009 (Fig 11b,d,f,h) consistent with other studies suggesting a weak-
541 ening over that period caused by density decreases in the Labrador Sea (Danabasoglu
542 et al., 2016; Robson et al., 2016, 2012). This weakening is not seen in the Ekman com-
543 ponent, but is seen in the multi-model mean minus the Ekman component (red line in
544 Fig 11f). The magnitude of weakening is of a similar magnitude to trends in the AMOC
545 at 45°N from 1995-2007 in an ensemble of forced ocean models (multimodel mean -0.15
546 Sv/year, Danabasoglu et al. (2016)) and a previous ensemble of reanalyses (multimodel
547 mean \sim -0.16 Sv/year Karspeck et al. (2017)). Most reanalyses also show a significant
548 weakening for the longer period 1993-2016 (not shown).

549 Recent observations by the OSNAP array have measured the AMOC in the sub-
550 polar gyre. This is across a line stretching from Newfoundland, Canada to the south-
551 ern tip of Greenland and then to Scotland and measures the AMOC in density space.
552 Since there are only 21 months of observations currently we do a comparison of monthly
553 values in Fig 13d. Those reanalyses for which this calculation was done show very sim-
554 ilar variability, with a minimum in winter 2014/15 followed by an increase in spring/summer
555 2015, and a gradual weakening to winter 2016. Although the timing of the variability
556 fits with the seasonal cycle of most reanalyses (Fig 13c), the magnitude of the observed
557 changes is much larger than the seasonal cycle: in particular the minimum in winter 2014/15
558 is unusually low compared to the rest of the period since 1993. We hypothesize that the
559 monthly variability since 2014 is wind-driven (though not Ekman driven, see Lozier et
560 al. (2019)), which could explain the ability of the reanalyses to reproduce it consistently.
561 Interannual to decadal changes (Fig 13b) are more diverse. Most of the reanalyses show
562 some coherence in variability since 2006, with a weakening in 2008/2009, increasing abruptly
563 around 2009/2010 (which is possibly associated with the strong negative NAO that caused
564 the weakening at 26.5°N (McCarthy et al., 2012; C. D. Roberts et al., 2013a)), then weak-
565 ening again in 2012. However prior to 2006 there is little consistency in the signals. We
566 note that the increase around 2010 is similar to that seen in the AMOC in depth space
567 at 50°N (Fig 11b,d,f), however the OSNAP section does not otherwise show the same
568 consistent interannual variability.

569 Many studies have shown relationships between the AMOC strength and the den-
570 sity in the Labrador Sea over decadal timescales (Jackson et al., 2016; C. D. Roberts,
571 Garry, & Jackson, 2013b). About half of the reanalyses show a weakening trend in the
572 0-500m LS density from 1993-2009 (although about half show little trend), and most show
573 a weakening trend in 1500-1900m density. Observational products agree that there was
574 a density decrease over this period at both depths. Most reanalyses also agree that there
575 was a weakening of M50, but there is no significant relationship found across the reanal-
576 yses between the trends in either 0-500m density or 1500-1900m density, and the trends
577 in M50 (Fig 14a,b). This suggests that either the sensitivity of the AMOC weakening
578 to the density weakening varies across the ensemble or that there is no direct relation-
579 ship within the reanalyses. This may be because aspects of the assimilation modify the
580 relationship. It is also possible, however, that there would be a stronger relationship with
581 a different density metric, for instance some models and reanalyses have shown a rela-
582 tionship with the GIN seas density or using a lagged correlation (Ba et al., 2014; Storto,
583 Masina, & Navarra, 2016). Recent observations of overturning in the subpolar gyre have
584 found that the majority of the overturning occurs to the east of Greenland, raising ques-
585 tions as to how relationships between the Labrador Sea density and AMOC strength should
586 be interpreted (Lozier et al., 2019).

587 Studies of decadal variability have shown lagged relationships of the AMOC at dif-
588 ferent latitudes, with the AMOC in the SPG preceding that at 26.5°N (Williams et al.,
589 2014; Yeager & Danabasoglu, 2014). We do not have sufficient years to examine corre-
590 lations between the two timeseries, however we note that Jackson et al. (2016) suggested
591 that the weakening of the SPG AMOC since the mid 90s was related to the later observed
592 weakening of the AMOC at 26.5°N . Hence we compare the magnitudes of weakening be-
593 tween these two events (Fig 14d), but see no relationship across reanalyses.

594 4.4 Gyre Circulation

595 Anomalies of the SPG and STG strengths are shown in Fig 15. These are defined
596 as the maximum of the barotropic streamfunctions over $60-30^{\circ}\text{W}$, $50-60^{\circ}\text{N}$ (SPG) and
597 $80-50^{\circ}\text{W}$, $25-38^{\circ}\text{N}$ (STG). For the SPG there is a weakening (positive trend in the stream-
598 function) up to 2009 seen in the ensemble average. All ensemble members show this pos-
599 itive trend which is significant in most of the members (Fig 15g). For the trend to 2016
600 GONDOLA100A disagrees with the rest of the ensemble in having a significant strength-

601 ening (negative trend). The weakening of the subpolar gyre from a maximum in the mid
602 90s has also been seen in many previous studies (Boning, Scheinert, Dengg, Biastoch,
603 & Funk, 2006; Danabasoglu et al., 2016; Lohmann et al., 2009). An index of subpolar
604 gyre strength based on observed sea surface heights (Häkkinen & Rhines, 2004) also shows
605 a weakening since the mid 90s, however modified definitions of the gyre index have shown
606 a partial recovery since 2010 (Foukal & Lozier, 2017; Hatun & Chafik, 2018).

607 There is also a temporary strengthening of the SPG around 2009-2010. This is likely
608 to be linked to the strong negative NAO that is associated with a weakening of the AMOC
609 at 26.5°N and a strengthening at 50°N. The STG in GLORYS2v4 is very weak between
610 1998 and 2004, leading to a large ensemble spread over that period. Most ensemble mem-
611 bers show a weakening of the STG from 1993-2016, however this is only significant in
612 a couple of members (Fig 15g).

613 Although most reanalyses agree that there was a weakening of the SPG and M50,
614 there is again no significant relationship across the ensemble (Fig 14c). A relationship
615 between the two has been seen in other studies (Ba et al., 2014; Boning et al., 2006; Dan-
616 abasoglu et al., 2016). Yeager (2015) show that this relationship is through the inter-
617 action of deep densities with the topography.

618 **4.5 Transports**

619 Heat transports at 26.5°N are strongly dominated by the overturning component
620 with little transport by the horizontal circulation component (Fig 16). This is in agree-
621 ment with observations and other modeling studies (Danabasoglu et al., 2016; Johns et
622 al., 2011; Msadek et al., 2013). We find strong correlations between the AMOC trends
623 over 2005-2015 and the trends in both overturning and total heat transports ($R > 0.86$,
624 $p < 0.01$, Fig 18a,b). The reanalyses also show strong correlations of the interannual
625 AMOC and heat transport timeseries within each reanalysis at 26.5°N (Fig 18e). Re-
626 gression coefficients of annual means in those reanalyses where the comparison is signif-
627 icant are between 0.04-0.08 PW/Sv with the observations being within this range (0.07
628 PW/Sv). A comparison with forced ocean models gives similar values (Danabasoglu et
629 al., 2016), and the regression coefficient when comparing trends (Fig 18b) is also within
630 this range (0.05 PW/Sv). This evidence all points to a strong relationship between the
631 AMOC at 26.5°N and the heat transport at this latitude.

632 We also note that there is some correspondence between periods where the heat
633 transports are high (1999, 2006-2008, 2012) with periods when there is an increase in
634 subtropical temperature, and periods where heat transports are low (2000, 2010-2013)
635 with periods of subtropical cooling (Fig 8a and 16a). Surface heat fluxes can also be im-
636 portant in changing the temperature of the region, and reanalyses also have changes in
637 heat from the assimilation of data. A rigorous examination of the heat budget across re-
638 analyses would require a comparison of assimilation terms, as well as surface fluxes, and
639 hence is difficult for a multi-model ensemble of reanalyses.

640 For freshwater transport, although there is a good relationship between the AMOC
641 and the overturning transport component at 26.5°N ($R = -0.92$, $p < 0.01$, Fig 18c),
642 the horizontal transport component also plays an important role in the variability and
643 strength of the freshwater transport, which prevents any clear relationship of the AMOC
644 with the total transport ($R = -0.28$, $p = 0.54$, Fig 18d).

645 At 50°N most of the variability and strength of the heat and freshwater transports
646 depends on the horizontal part, rather than the overturning part of the transport (Fig
647 17). However we note that the thermohaline circulation, which represents the circula-
648 tion resulting from water mass transformation, has a strong horizontal component in the
649 subpolar region, rather than being predominantly in the overturning component (Yea-
650 ger, 2015).

651 There is a clear weakening seen in the horizontal and total heat transport at 50°N
652 from the mid 90s (see Fig 17). Strong transports of heat and freshwater near the start
653 of the period are consistent with the warming and salinification seen in the subpolar gyre,
654 and weaker transports towards the end of the period are consistent with a cooling and
655 freshening (Fig 8). We note that surface fluxes also play a role and that the recent cool-
656 ing since 2014 in the subpolar gyre has been linked to surface cooling (Grist et al., 2016;
657 Josey et al., 2018).

658 Although there is a significant correlation between the trends of AMOC and over-
659 turning transport of heat at 50°N ($R = 0.83$, $p = 0.02$), this is not a significant con-
660 tribution to the trend in total heat transport (Fig 17). Indeed there is no significant re-
661 lationship between the trends in AMOC or SPG and trends in total heat or freshwater
662 transports at 50°N (not shown). In most individual reanalyses there are significant cor-

663 relations between the total heat transport timeseries and both the AMOC and SPG time-
664 series, but this is likely because these timeseries all have trends (Fig 18e).

665 **5 Discussion and conclusions**

666 We have presented results from examining the mean state and variability of the North
667 Atlantic since 1993 from an ensemble of global ocean reanalyses. The results here are
668 relevant to those using and developing the reanalyses and those wanting to understand
669 how and why the North Atlantic has changed recently. We focus our discussion and con-
670 clusions on the questions introduced in the introduction.

671 **5.1 Where is there agreement or disagreement across reanalyses?**

672 Reanalyses are able to capture many aspects of the dynamics in the North Atlantic.

673 In particular:

- 674 • Although there is large disagreement among reanalyses in the Labrador Sea mixed
675 layer depth initially, this improves in time. This is likely to be because of greater
676 observational constraints later in the period (eg the introduction of Argo in the
677 mid 2000s).
- 678 • There is consistency across the ensemble of variability in the AMOC at both 26.5
679 and 50°N (and agreement of the former with independent observations). This is
680 in contrast with a previous study (Karspeck et al., 2017) that found little agree-
681 ment of reanalyses over an earlier, more observation-sparse period. There is also
682 agreement of monthly variability with new observations of overturning in the sub-
683 polar North Atlantic.
- 684 • At 26.5°N the reanalyses mostly agree with the independent observational esti-
685 mates of mean AMOC strength. However they underestimate the ocean heat trans-
686 port (OHT) per Sverdrup of volume transport, despite having a strong correla-
687 tion between AMOC and OHT. This discrepancy has previously been seen in ocean
688 models (Danabasoglu et al., 2014).
- 689 • The reanalyses using NEMO at 0.25 and 1/12° have more intense Gulf Streams
690 and stronger transports of heat and freshwater from 30-50°N. These differences
691 may be because they have higher horizontal resolutions (eddy-permitting and eddy-
692 resolving).

693 • NorCPM-v1 is an outlier in the mean comparisons because it uses anomaly assim-
694 ilation. GECCO2 is also an outlier in several comparisons, particularly of variabil-
695 ity. This may be because it was run over several short (5 year) windows. ORAS5
696 has a large change in Labrador Sea density and AMOC strength from 1996-2000
697 which is associated with extra buoyancy loss caused by SST nudging and sparse
698 in-situ observations in the early period (Tietsche, personal comm).

699 **5.2 Can we learn what makes reanalyses good at specific processes?**

700 • A greater availability of observations can improve the representation of processes.
701 In particular mixed layer depths within the Labrador Sea improve over the lat-
702 ter half of the period studied. There is also a greater agreement among the reanal-
703 yses (and with observations from 2004) of the variability of AMOC strength at
704 26.5N than in a previous study looking at an earlier, more observation-sparse pe-
705 riod.

706 • Some reanalyses have density variability in the deep Labrador Sea that is driven
707 by salinity, rather than temperature, variability. This may affect their ability to
708 capture the observed decline and may have an impact on dynamics. This suggests
709 that more deep observations, such as deep Argo, are needed.

710 • Eddy-permitting and resolving resolution, such as used in the NEMO-based re-
711 analyses, can strengthen western boundary currents and transports at mid-latitudes.

712 • ECCO V4 R3 uses a 4DVar scheme where adjustments are made to parameters
713 such as surface forcing and ocean mixing rather than directly modifying temper-
714 ature and salinity through increments. It shows similar variability to other (non
715 4DVar) reanalyses, and to some independent observations. This improves our con-
716 fidence that both 4DVar and non-4DVar schemes can produce reasonable results.
717 However ECCO V4 R3 does have the wrong density drivers and trends in the deep
718 Labrador Sea water, possibly because the assimilation scheme does not directly
719 affect deep properties and instead changes much be subducted or vertically mixed
720 from the surface, or changes can be made by modifications of the mixing itself (for
721 instance by changes in winds). We do note, though, that 4DVar has advantages
722 in that it avoids direct adjustments of water masses, and is therefore more dynam-
723 ically consistent.

5.3 Can these reanalyses improve our understanding of the dynamics in the North Atlantic ocean?

- Results support the subpolar picture of a decrease in Labrador Sea density, and a weakening SPG and AMOC at 50°N over the period (attributed by other studies to decadal-multidecadal variability). Heat and freshwater transports also show a decline. The strong (weak) transports in 1993-2005 (2005-2016) are consistent with an increase (decrease) in temperature and salinity.
- Results support the subtropical picture of strong interannual variability, with a gradual warming and salinification consistent with anthropogenic climate change. A strong relationship between the AMOC and the heat transport at 26.5 °N is found, which in turn can impact the subtropical heat content.
- Reanalyses with denser mean upper Labrador Sea densities have a stronger mean AMOC at 50°N. No relationships are found between the trends across the reanalyses. There is also no relationship found between the AMOC at 26.5 and 50°N, either in mean strength or variability.
- Although there is a strong relationship between the AMOC and heat transport at 26.5°N, there is no clear relationship across the reanalyses between the heat transport at 50°N and the SPG or AMOC transports (either for the mean or variability).
- Reanalyses mostly agree that the AMOC at 26.5°N showed a weakening from 1999-2001, followed by a strengthening from 2001-2006 and then a weakening from 2006-2013. This suggests that the observed weakening (since 2004) is part of interannual-decadal variability.
- Reanalyses mostly agree that the AMOC at 50°N has interannual variability from the Ekman component superimposed on a more gradual weakening from the mid 90s.
- Reanalyses also compare well with the OSNAP section, suggesting that they may be useful tools to further understand the variability and its cause

Although many relationships found in modeling studies are not found to hold across these reanalyses, it does not mean that those relationships do not hold in reality. For example, we see trends from the mid 90s in many variables in the subpolar gyre region. These variables could be physically related and show correlations of timeseries, however

756 the strengths and timing of these relationships could differ across reanalyses. Hence re-
757 lationships between trends are not found. It is also possible that stronger relationships
758 would be found with different metrics, time periods or lags. In reanalyses it is also pos-
759 sible that relationships can be obscured or changed by spatial or temporal variations in
760 the quality of the observational constraints. Hence to properly explore mechanisms us-
761 ing a reanalysis, a good understanding is required of whether relevant processes are phys-
762 ically consistent, or whether there are spurious impacts from the assimilation (Storto et
763 al., 2019).

764 Nevertheless, reanalyses are promising tools to examine recent climate variability
765 alongside free running ocean models (which can experience biases) and observations (which
766 are temporally and spatially sparse). Reanalyses cannot be a replacement for observa-
767 tions: in particular a good observational coverage is necessary for constraining reanal-
768 yses. Independent observations, such as the AMOC transports calculated by the RAPID
769 and OSNAP sections, are also independent checks. We note that although reanalyses are
770 able to realistically simulate many aspects of the AMOC at 26.5°N , they cannot sim-
771 ulate important details, such as the different AMOC components. Hence it is important
772 to continue these observational campaigns, along with developing ocean reanalyses, in
773 order to understand and monitor the ocean.

Table 1: Acronyms used

Acronym	Full name	Notes
3DVar	Three dimensional variational analysis	technique
4DVar	Four dimensional variational analysis	technique
AER	Atmospheric and environmental research	institute/group
AMOC	Atlantic Meridional Overturning Circulation	physical quantity
BBL	Bottom boundary layer	technique
BCCR	Bjerknes centre for climate research	institute/group
BSF	Barotropic streamfunction	physical quantity
CICE	Sea ice model	model
CLIVAR	Climate Variability and Predictability	institute/group
CMCC	Centro Euro-Mediterraneo sui Cambiamenti Climatici	institute/group
CORA	Coriolis ocean dataset for reanalysis	ocean observational product
ECMWF	European Center for Medium-range Weather Forecasting	institute/group
EN4	EN4	ocean observational product
EnKF	Ensemble Kalman filter	technique
ERA	ECMWF reanalysis	atmospheric reanalysis product
FGAT	First guess at appropriate time	technique
GCM	Coupled general circulation model	model
GFDL	Geophysical Fluid Dynamics Laboratory	institute/group
GODAE	Global Ocean Data Assimilation Experiment	institute/group
GSOP	Global synthesis and observations panel	institute/group
JMA	Japan meteorological agency	institute/group
JPL	Jet propulsion laboratory	institute/group
JRA	Japan reanalysis	atmospheric reanalysis product
KF	Kalman filter	technique
LIM	Louvain-la-Neuve Sea Ice Model	model
LS	Labrador Sea	physical quantity
M26	AMOC strength at 26.5N	physical quantity
M50	AMOC strength at 50N	physical quantity
MICOM	Miami Isopycnal Coordinate Ocean Model	model
MIT	Massachusetts Institute of Technology	institute/group

MITgcm	MIT general circulation model	model
MLD	mixed layer depth	physical quantity
MOCHA	Meridional overturning circulation and heat-flux array	ocean observational product
MOM	Modular Ocean Model	model
MRI	Meteorological Research Institute	institute/group
MRI.COM	Meteorological Research Institute Community Ocean Model	model
NAO	North Atlantic Oscillation	physical quantity
NCEP	National center for environmental prediction	atmospheric reanalysis product
NEMO	Nucleus for European Modelling of the Ocean	model
NOAA	National Oceanic and Atmospheric Administration	institute/group
OBP	Ocean bottom pressure	physical quantity
OFWT	Ocean fresh water transport	physical quantity
OHC	Ocean heat content	physical quantity
OHT	Ocean heat transport	physical quantity
OI	Optimal interpolation	technique
ORA	Ocean Reanalysis	institute/group
OSNAP	Overturning in the subpolar north atlantic project	ocean observational product
RAPID	Observational array for measuring AMOC at 26.5N	ocean observational product
S	salinity	physical quantity
SIC	Sea ice concentration	physical quantity
SIS	GFDL Sea Ice Simulator	model
SIT	Sea ice thickness	physical quantity
SPG	Subpolar gyre	physical quantity
SSH	Sea surface height	physical quantity
SSS	Sea surface salinity	physical quantity
SST	Sea surface temperature	physical quantity
STG	subtropical gyre	physical quantity
T	temperature	physical quantity

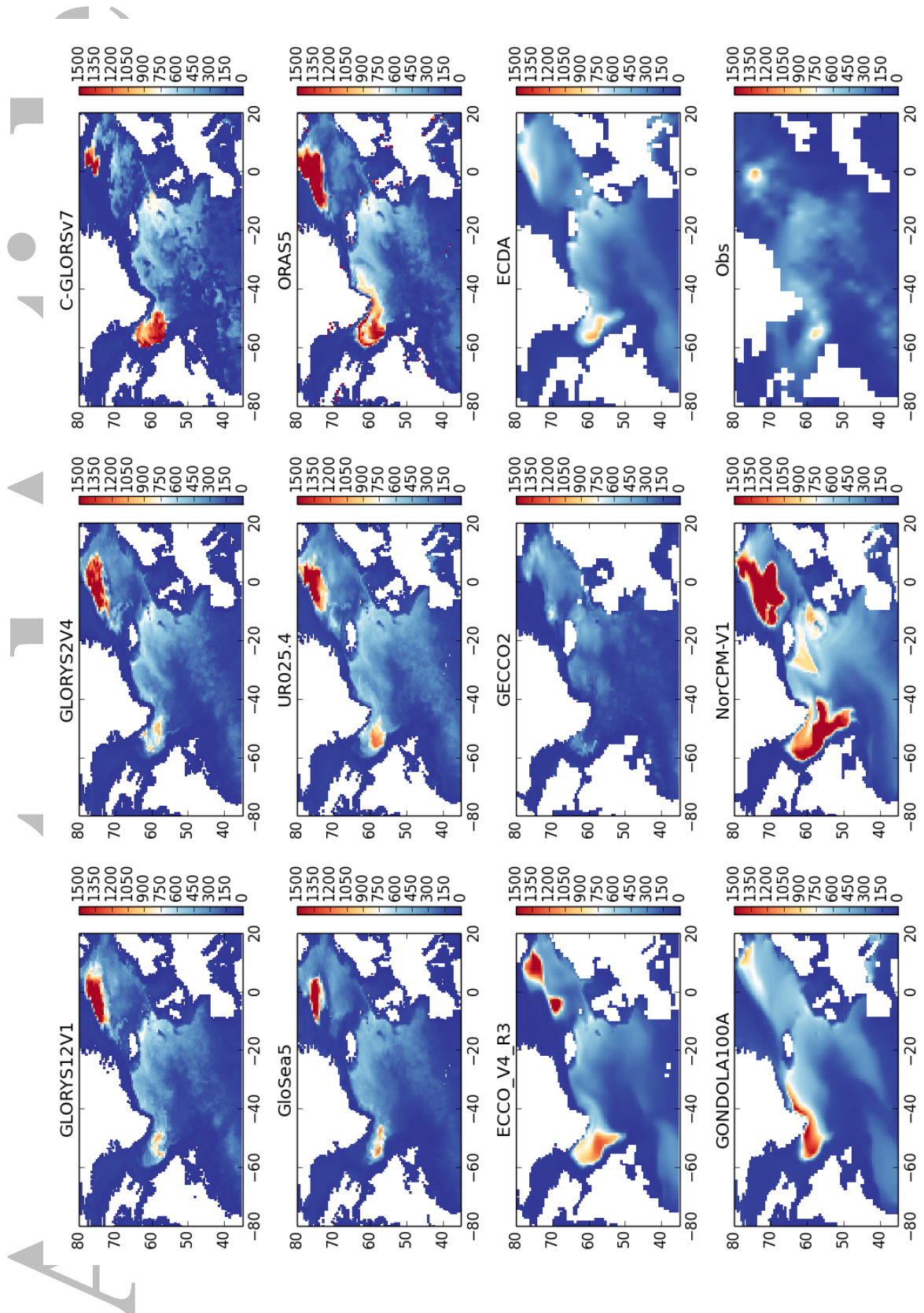
Project Name	Resolution	Model	Year	Method	Reference									
C-GLORSv7	ECDA3	GFDL/NOAA	1x1/3°	50 z-levels	10 m	Y	MOM4/SIS	1970–2017	cold start	NCEP RA1	EnKF	T, S, SST	None	Chang, Zhang, Rosati, Delworth, and Stern (2013); S. Zhang, Harrison, Rosati, and Wittenberg (2007)
CECCO2	Hamburg University	1x1/3-1°	50 z-levels	10 m	Y	MITgcm	NEMO3.1/LIM2	1948–2017	optimized	NCEP RA1	4DVAR adjoint	T, S, SSH, SST, SSS	None	Kohl (2015)
GLORYS2v4	Mercator Ocean	0.25°	75 z-levels	~1 m	N	NEMO3.1/LIM2		1992–2016	spinup	ERA-Interim	reduced order KF + 3DVAR	T, S, SSH, SST	None	Ferry et al. (2012)
GloSea5	UK Met Office	0.25°	75 z-levels	~1 m	N	NEMO3.4/CICE4.1		1989–2017	spinup	ERA-Interim	3DVAR	T, S, SSH, SST, SIC	SSS (Haney flux). Weak relaxation to T,S climatology	Blockley et al. (2014); Jackson et al. (2016); MacLachlan et al. (2015)
ECCO V4 R3	MIT/JPL/AER	1x1/3-1°	50 z-levels	10m	Y	MITgcm		1992–2015	optimized	ERA-Interim	4DVAR adjoint	T, S, SSH, SST, SSS, SIC, OBP	None	Forget et al. (2015); Fukumori et al. (2017)
ORAS5	ECMWF	0.25°	75 z-levels	~1 m	N	NEMO3.4/LIM2		1979–2017	spinup	ERA-Interim, NWP after 2015	3DVAR FGAT	T, S, SSH, SST, SIC	SSS. Weak relaxation to T,S climatology	Zuo, A, Tietze, Moegenstern, and Mayer (2019)
UR025.4	University of Reading	0.25°	75 z-levels	~1 m	N	NEMO3.2/LIM2		1989–2010	cold start	ERA-Interim	OI	T, S, SSH, SST, SIC	None	Valdivieso, Haines, Zuo, and Lea (2014)
GLORYS12v1	Mercator Ocean	1/12°	50 z-levels	~1 m	N	NEMO3.1/LIM2		1992–2016	spinup	ERA-Interim	reduced order KF + 3DVAR large scale bias correction to in-situ T, S SST	None	Lellouche et al. (2018)	
GONDOLA100A	MRI/JMA	1x1/3-0.5°	60 z-levels +BBL	~1m	Y	MRI.COMv4.2		19582015	Jan 2000 reanalysis JRA55-do v1.3		3DVar + robust diagnostic	T, S, SSH, SST, SIC	T,S climatology	Toyoda et al. (2016)
GLORYS12v1	Mercator Ocean	1/12°	50 z-levels	~1 m	N	NEMO3.1/LIM2		1992–2016	spinup	ERA-Interim	reduced order KF + 3DVAR large scale bias correction to in-situ T, S SST	None	Lellouche et al. (2018)	

Table 2. Description of reanalyses. 1) Notation in columns 3,6,10 of row 2 implies a zonal resolution of 1° and a meridional resolution varying from 0.5 or 1° down to 1/3° near the equator.

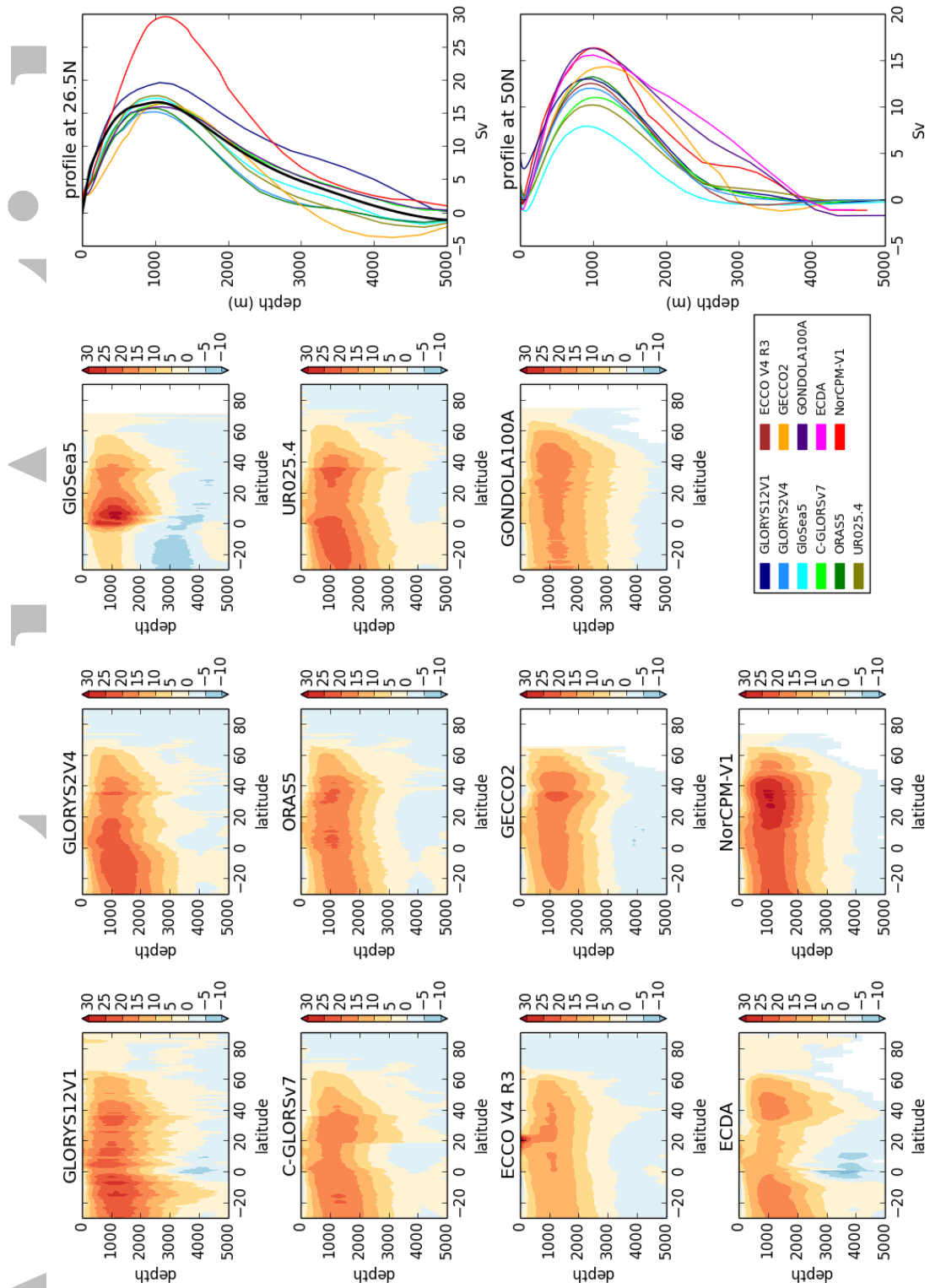
Acknowledgments

This work was initiated through the EU COST-EOS-1402 project which supported the development of this paper by funding project meetings, both in person and virtual. We would like to thank Aida Azcarate for organizing the funding for the meetings and would like to thank Martha Buckley, Gokhan Danabasoglu and Simon Josey for useful discussions. Jackson and Zuo were funded, and Storto partially funded, by the Copernicus Marine Environment Monitoring Service (CMEMS: 23-GLO-RAN). Haines and Robson acknowledge funding under the NERC RAPID projects RAMOC and DYNAMOC respectively, and Robson also acknowledges funding from the ACSIS project. Mignac was supported for PhD scholarship by the CAPES Foundation, Ministry of Education of Brazil (Proc. BEX 1386/15-8). Forget acknowledges support from the Simons Foundation (549931) and the NASA IDS program (6937342). Work by Piecuch was carried out under the ECCO project, funded by the NASA Physical Oceanography, Cryospheric Science, and Modeling, Analysis and Prediction programs. Wilson was funded by the NERC UK-OSNAP project (NE/K010875.1) as part of the international OSNAP programme. NorCPM-v1 reanalysis was co-funded by the Center for Climate Dynamics at the Bjerknes Center, the Norwegian Research Council under the EPOCASA (229774/E10) and SFE (270733) research projects, the NordForsk under the Nordic Centre of Excellence (ARCPATH, 76654), and the Trond Mohn Foundation under the project number BFS2018TMT01. NorCPM-v1 reanalysis received a grant for computer time from the Norwegian Program for supercomputer (NOTUR2, project number NN9039K) and a storage grant (NORSTORE, NS9039K).

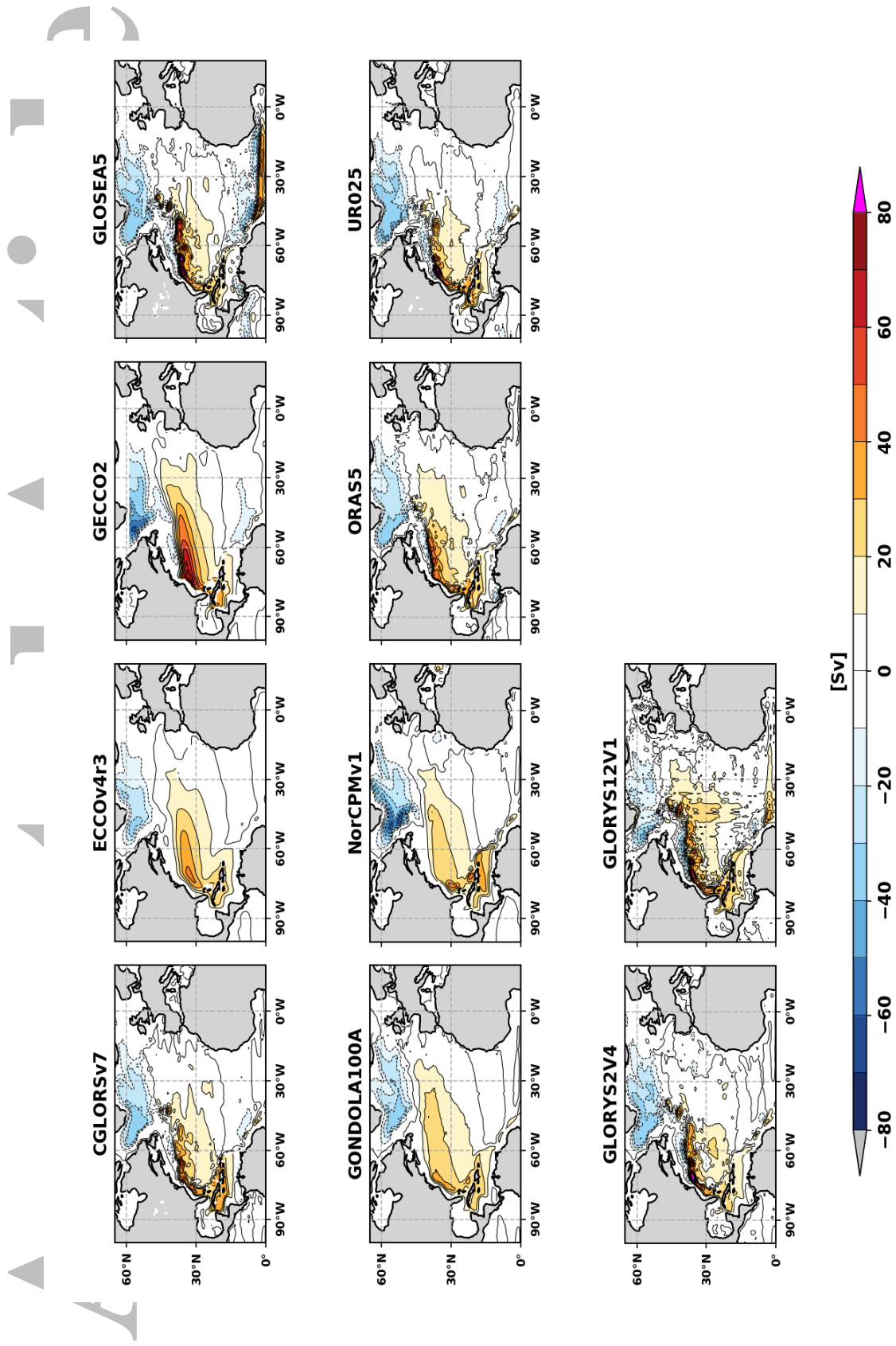
Data for the figures is available to download from <https://doi.org/10.5281/zenodo.2598509>. Data from some reanalysis products are available to download from <http://marine.copernicus.eu/services-portfolio/access-to-products/> under product names GLOBAL_REANALYSIS_PHY_001_025 (GLORYS2v4), GLOBAL_REANALYSIS_PHY_001_026 (C-GLORSv7, GLORYS2v4, GloSea5 and ORAS5) and GLOBAL_REANALYSIS_PHY_001_030 (GLORYS12V1).



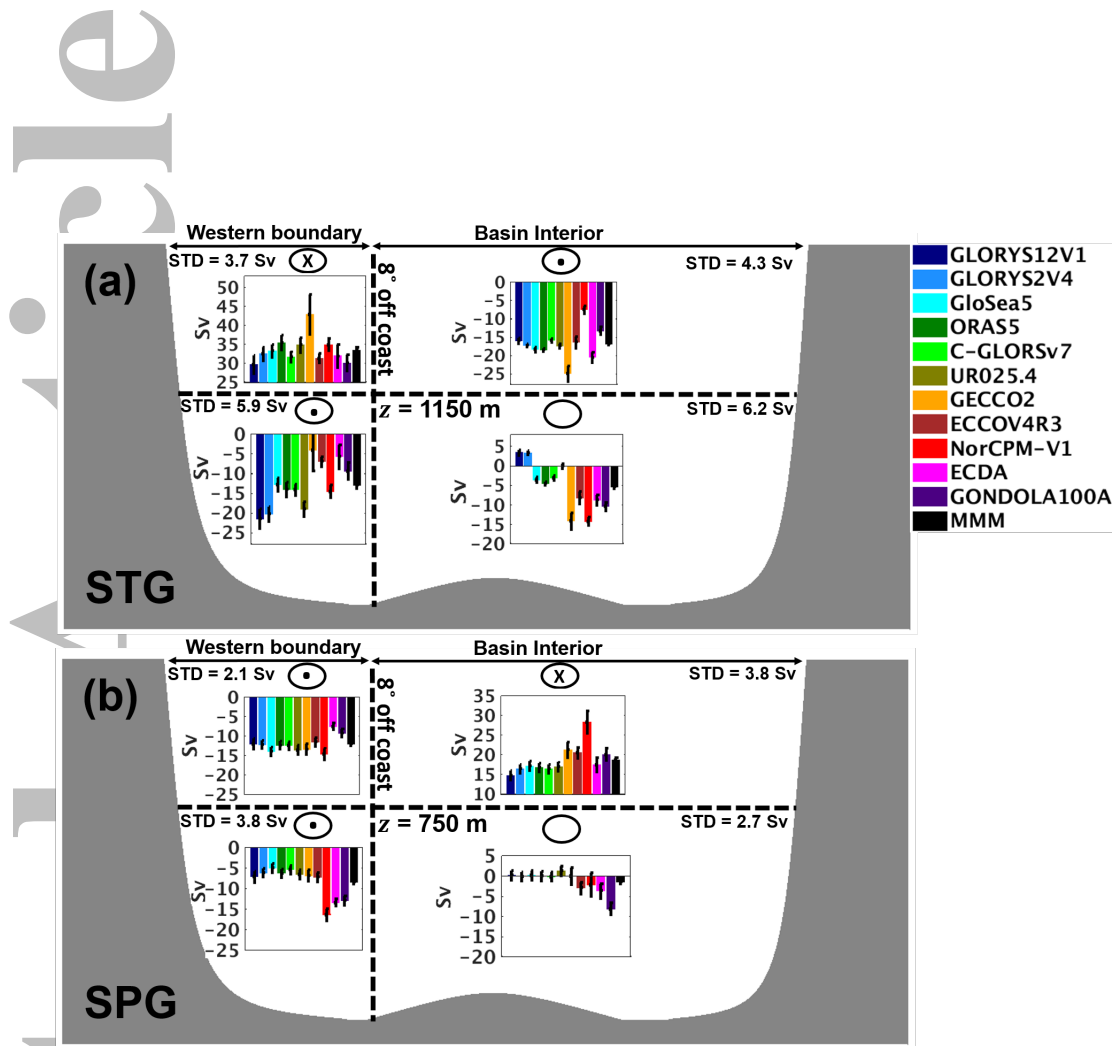
776 **Figure 1.** March mean (2004-2010) mixed layer depth (m) defined as the depth at which the
 777 density differences from the surface is 0.03 kg/m^3 (calculated from monthly mean density fields).
 778 The observational data set is the March mixed layer depth from de Boyer-Montegut et al. (2004).



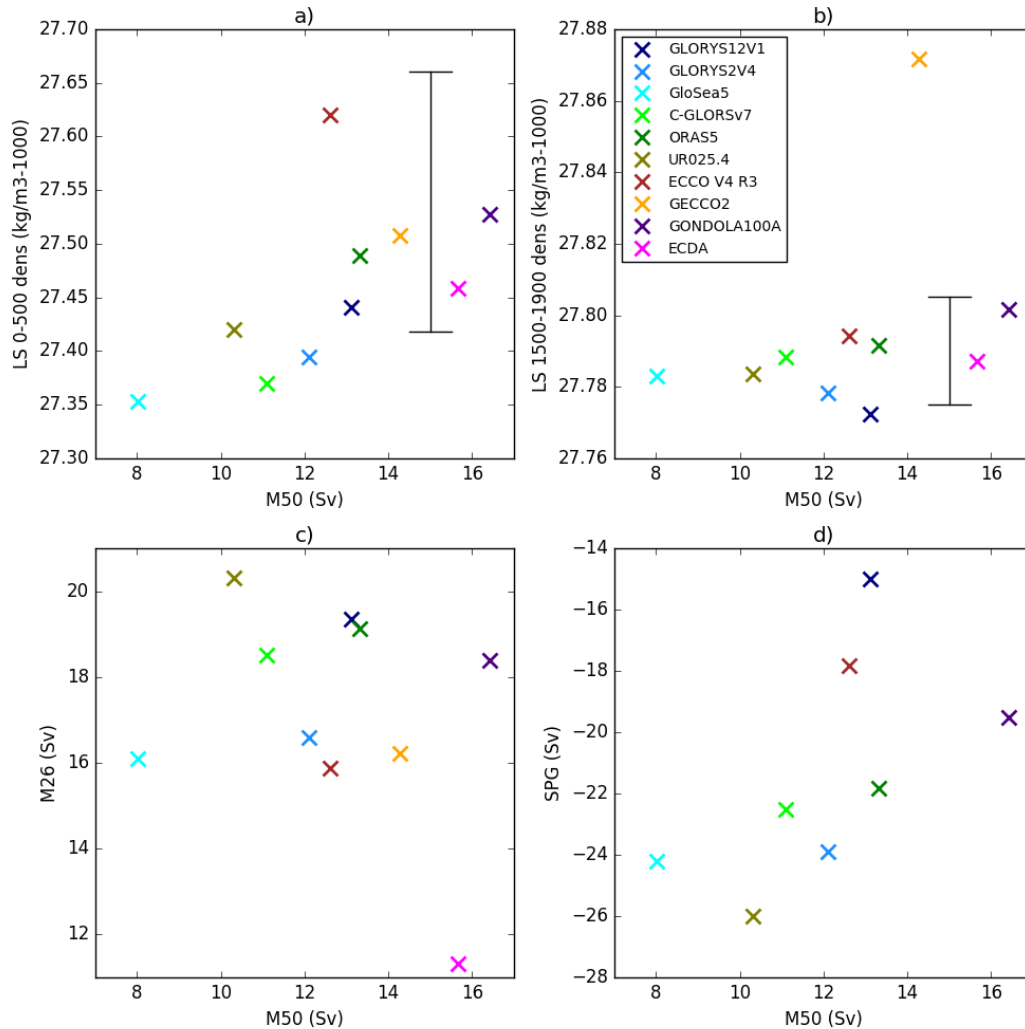
779 **Figure 2.** AMOC streamfunctions (from velocities) and profiles at 26.5°N (calculated using
 780 the RAPID methodology) and 50°N (from velocities). Units are Sverdrups ($Sv = 10^6 m^3/s$).
 781 Profiles use the time period 2004-2015 to agree with the observations, though the streamfunctions
 782 use the standard climatology period (1993-2010). Note that NorCPM-v1 is an outlier because it
 783 uses anomaly assimilation and hence the mean state is not constrained.



784 **Figure 3.** Barotropic streamfunctions (Sv) referenced to zero at the eastern boundary. Note
 785 that NorCPM-v1 uses anomaly assimilation and hence the mean state is not constrained.



786 **Figure 4.** 4-box model of the volume transports divided into upper, lower, deep western
 787 boundary and interior flows for (a) the subtropical gyre (26°N-40°N), and (b) the subpolar gyre
 788 (50°N-65°N). Units are Sv. 8° off the coast is chosen to separate the western boundary and in-
 789 terior, and the ensemble mean AMOC depth is used to separate the upper and lower limbs of
 790 the circulation for each region. The black error bars represent the uncertainty due to the varying
 791 AMOC depth between the models by using the standard deviation of the ensemble AMOC depth.
 792 The circles with dots correspond to flows going out of the page whereas the crosses represent
 793 flows going into the page. The circles without symbols mean that there is no consensus between
 794 the products about the direction of the flow. Note that NorCPM-v1 is an outlier because it uses
 795 anomaly assimilation and hence the mean state is not constrained.

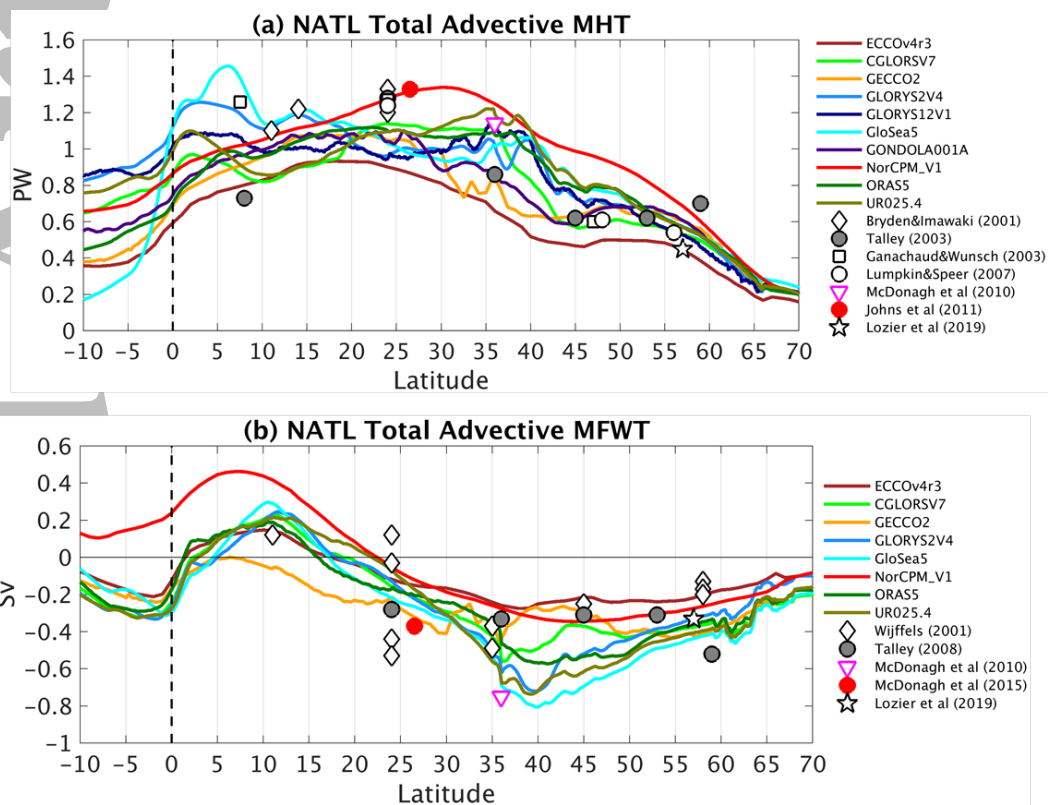


796 **Figure 5.** Comparison of the mean strengths of different variables across reanalyses (see
 797 labels). This includes the AMOC strength at 26.5°N and 50°N (M26,M50), the density in the
 798 Labrador Sea over 0-500m and 1500-1900m (over the region 75-40°W and 50-65°N), and the SPG
 799 strength. The black bars in the upper plots show the Labrador Sea densities from the EN4 and
 800 CORA observational estimates (with an arbitrary x value of M50=15Sv), with the difference in-
 801 dicated by observational uncertainty. Note that NorCPM-v1 is not included in this analysis because
 802 it uses anomaly assimilation and hence the mean state is not constrained.

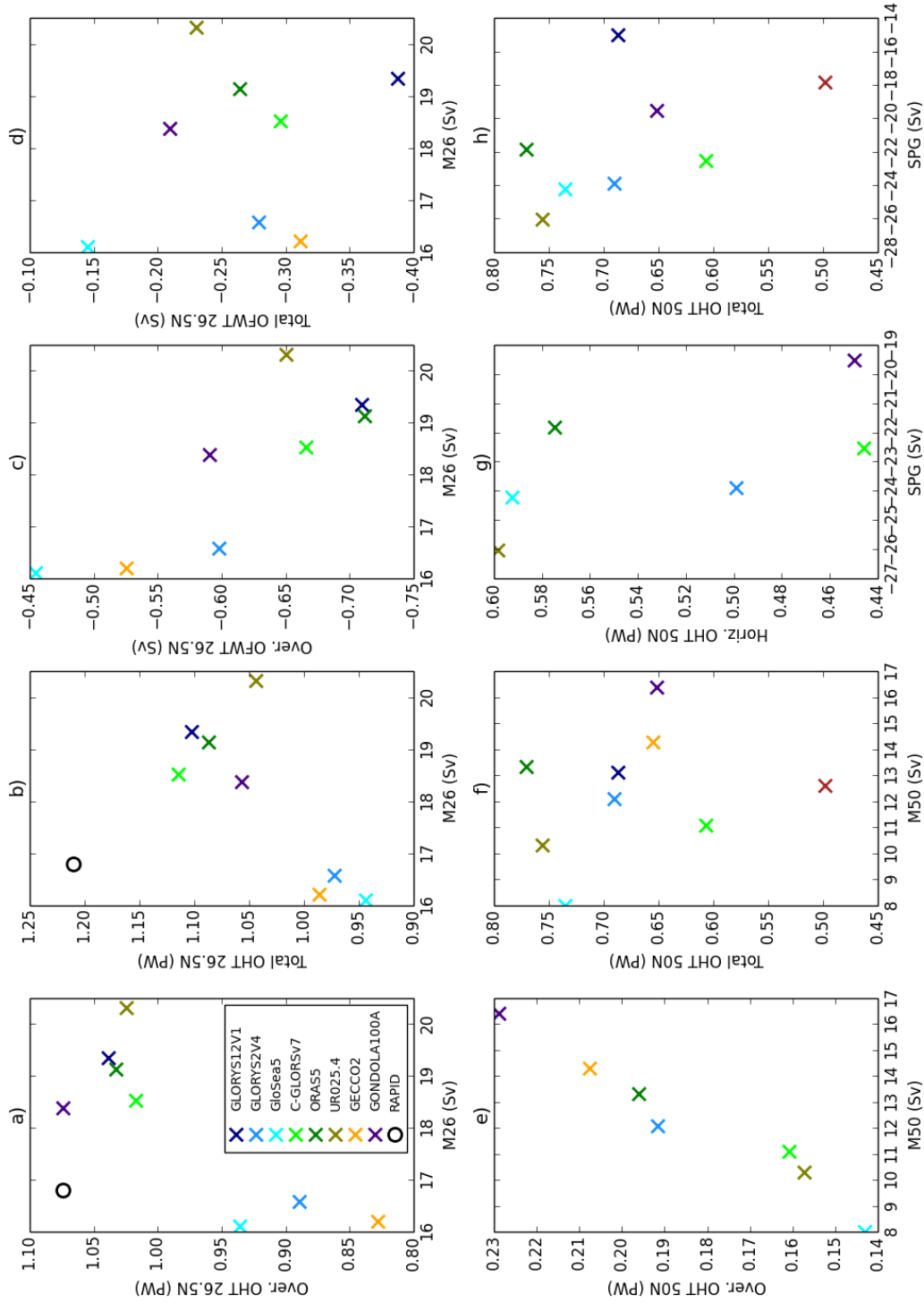
Article

Figure 6

Accepted

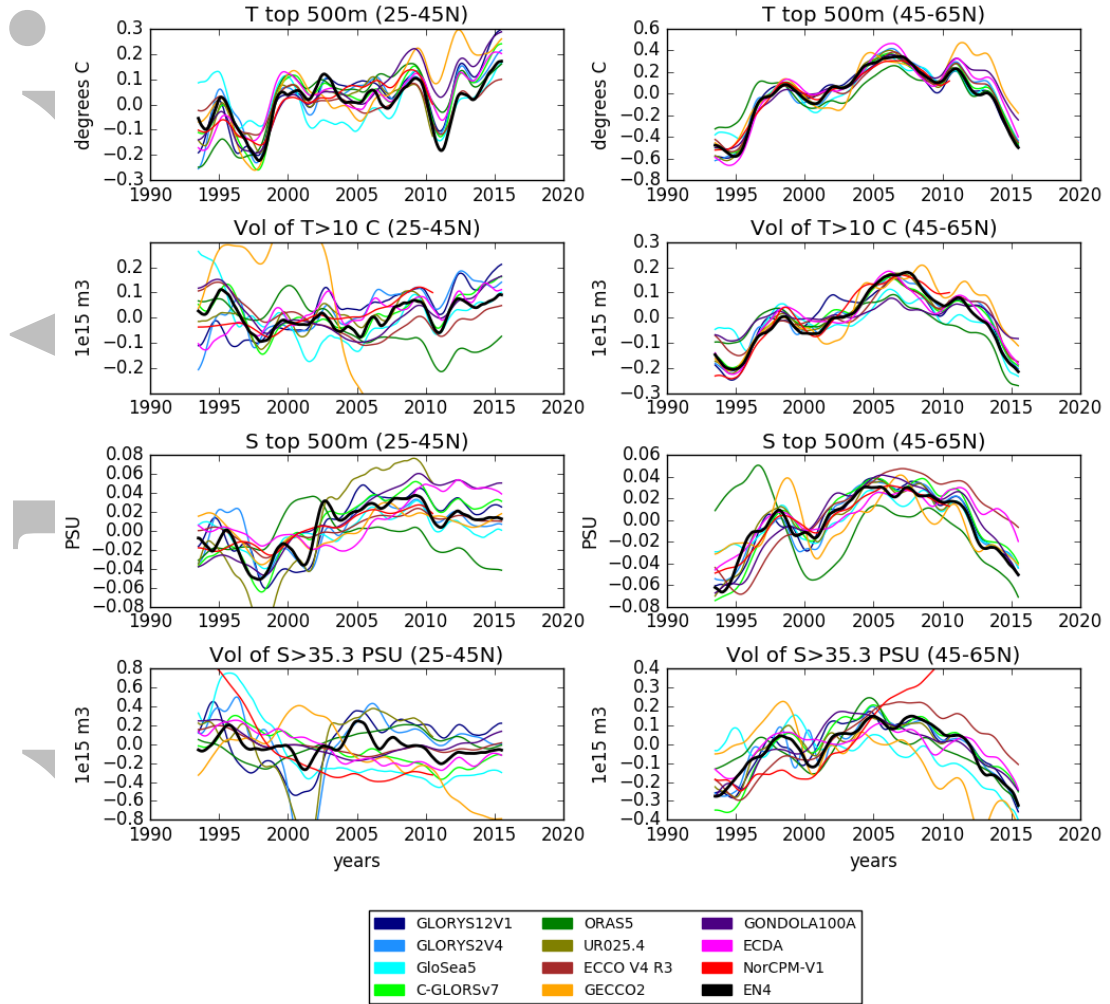


803 **Figure 6.** Mean meridional heat (top, in PW) and freshwater (bottom, in Sv) transports
 804 as a function of latitude. Also shown are observational measurements as symbols. Note that
 805 NorCPM-v1 is an outlier because it uses anomaly assimilation and hence the mean state is not
 806 constrained.



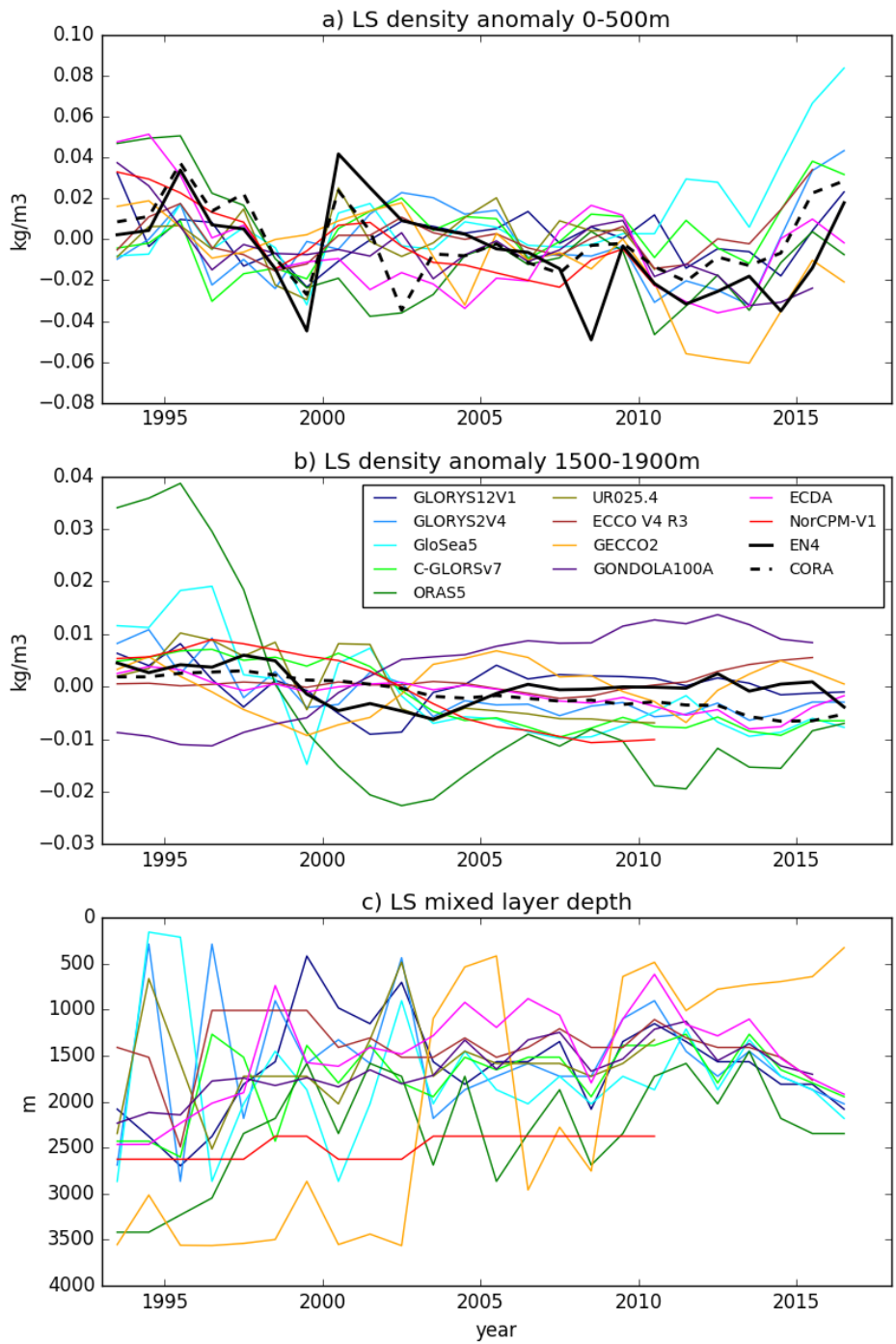
807 **Figure 7.** Comparison of the mean strengths of different variables across reanalyses (see labels).
 808 This includes the AMOC strength at 26.5°N and 50°N (M26,M50), the SPG strength and
 809 ocean heat and freshwater transports (OHT, OFWT). For the transports we also show the total
 810 transport and the overturning and horizontal components. Note that NorCPM-v1 is not included
 811 in this analysis because it uses anomaly assimilation and hence the mean state is not constrained.

icle

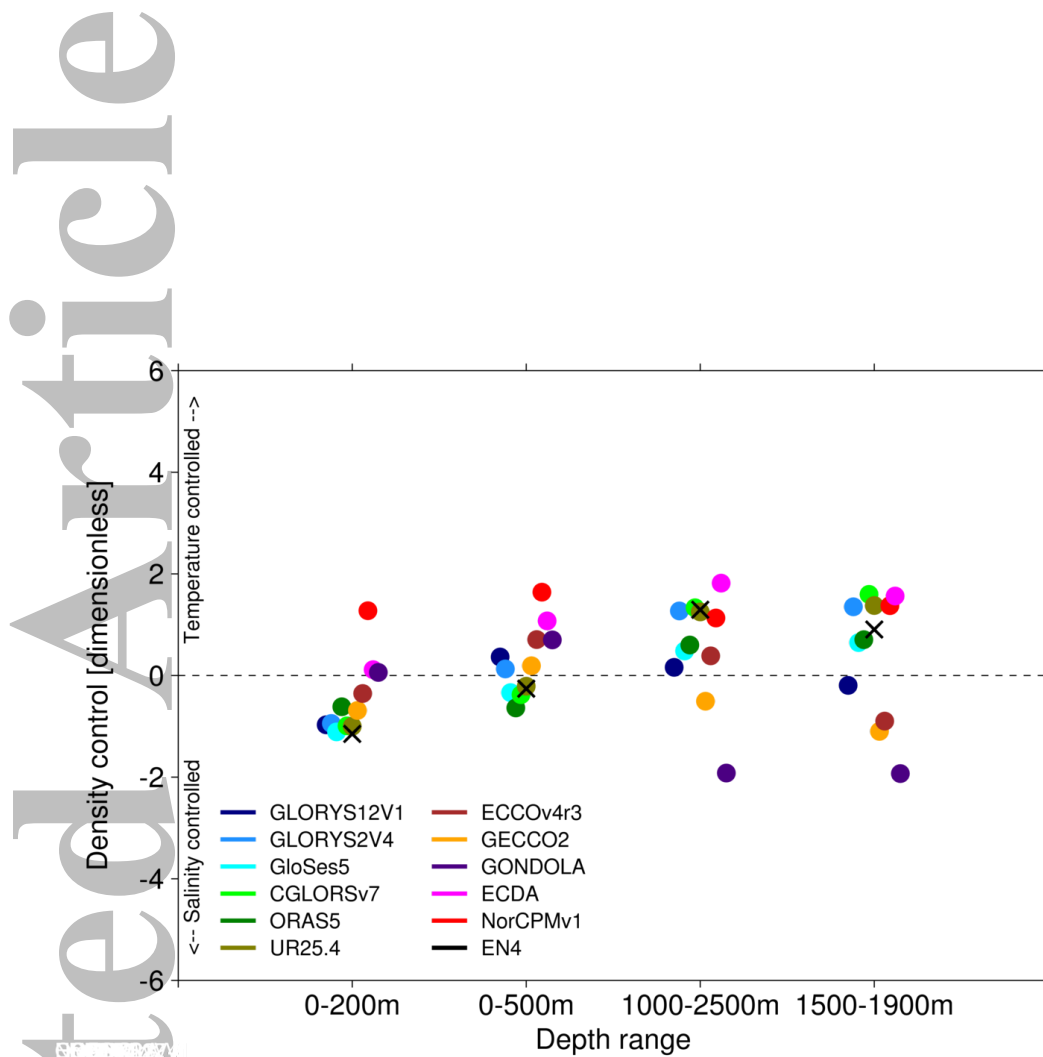


812 **Figure 8.** Anomalies of temperature (top row) in °C and salinity (third row) in PSU over the
 813 top 500m. Also shown is the volume of water (in m³) where T>10°C (second row) or S>35.3psu
 814 (bottom row). Left panels are for regions 25-45°N in the Atlantic and right panels for regions
 815 45-65°N. All timeseries are anomalies with a 12 month running mean applied.

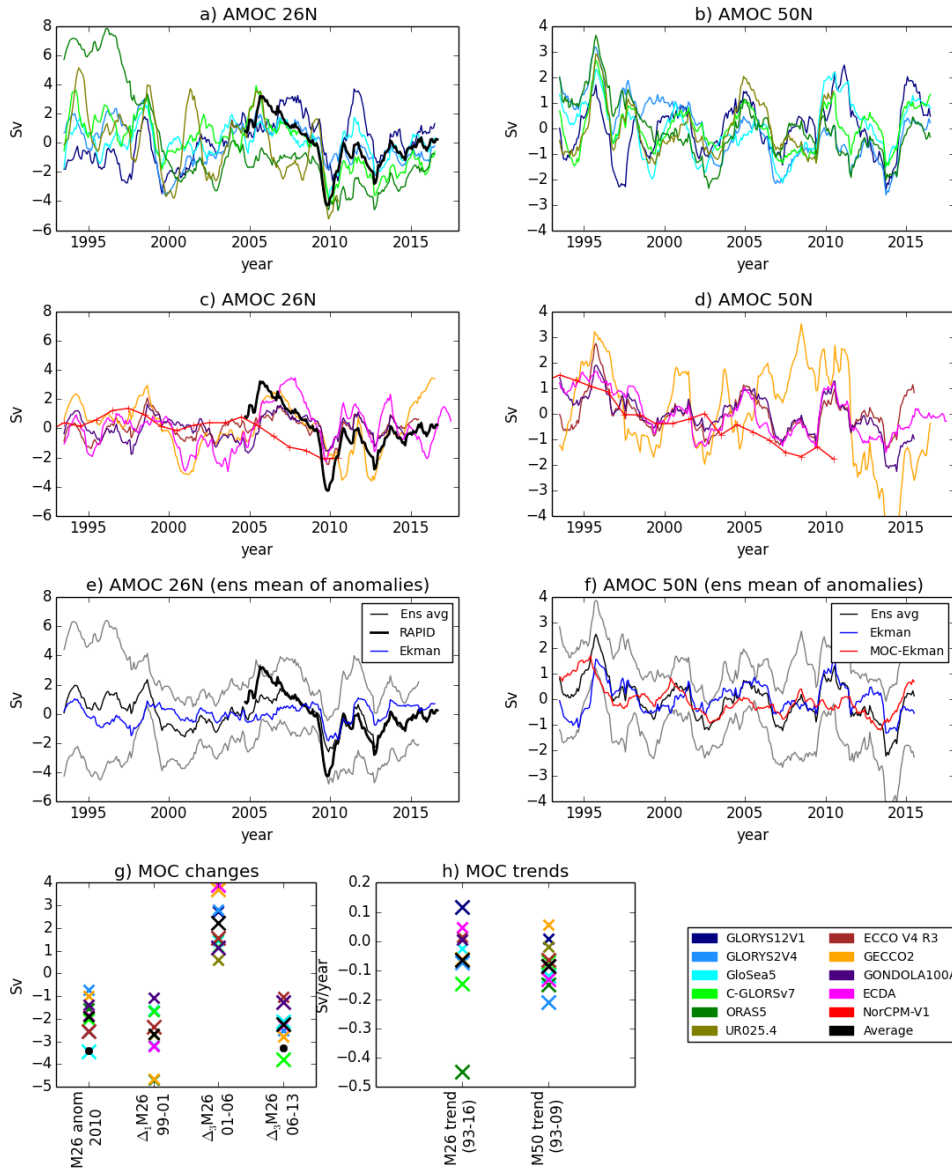
ACC



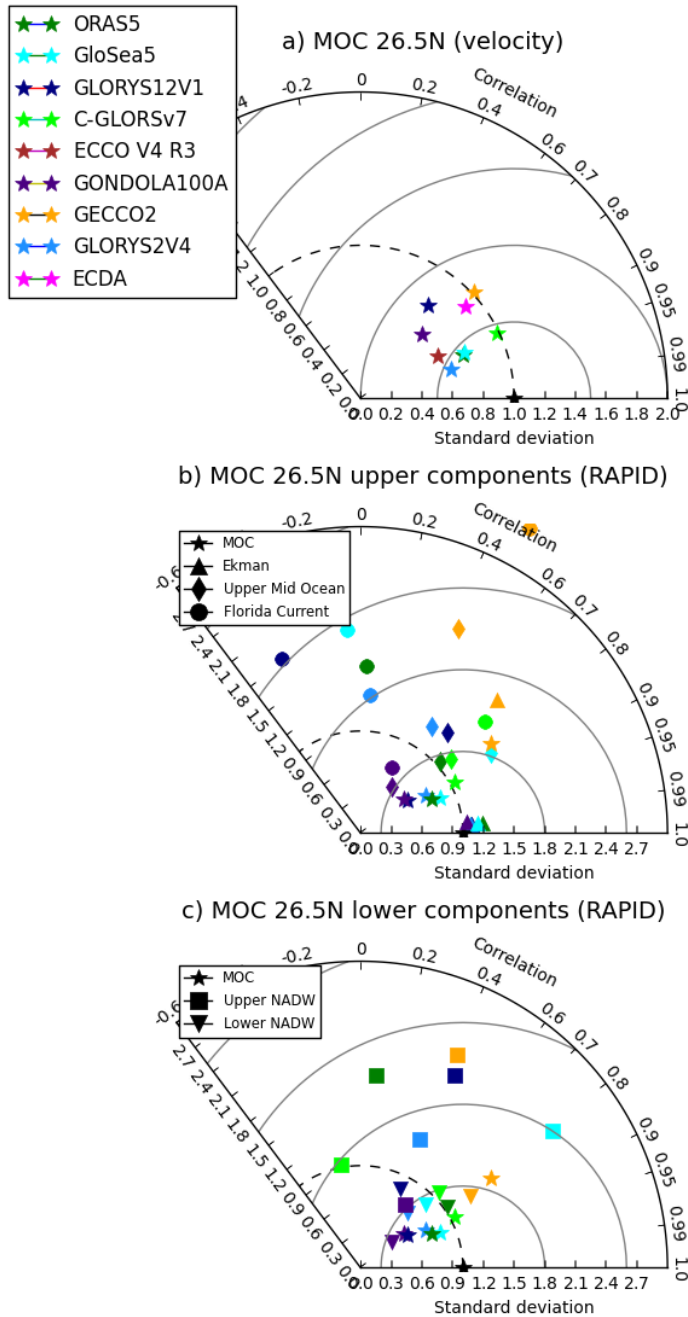
816 **Figure 9.** Time series of Labrador Sea density anomalies averaged over a) 0-500m or b)
 817 1500-1900m and the region 75-40°W and 50-65°N. c) The maximum mixed layer depth over the
 818 Labrador Sea (measured as the maximum over the region and over the year of mixed layer depths
 819 defined as the depth at which the monthly mean density differs by 0.03 kg/m³ from that at the
 820 surface



821 **Figure 10.** The relative strength of temperature or salinity in controlling density anomalies
 822 in the western subpolar North Atlantic. Positive values show density anomalies are dominated by
 823 temperature, whereas negative shows density anomalies are dominated by salinity. The density
 824 control metric is the difference between rT and rS , where rT (rS) is the correlation coefficient
 825 between the density resulting from changes in temperature (salinity) only (ie with the other vari-
 826 able constant), and the full density timeseries (Menary et al., 2016). Density drivers have been
 827 calculated for four different depth ranges (x-axis). The black cross shows the values from the
 828 EN4 observational analysis.

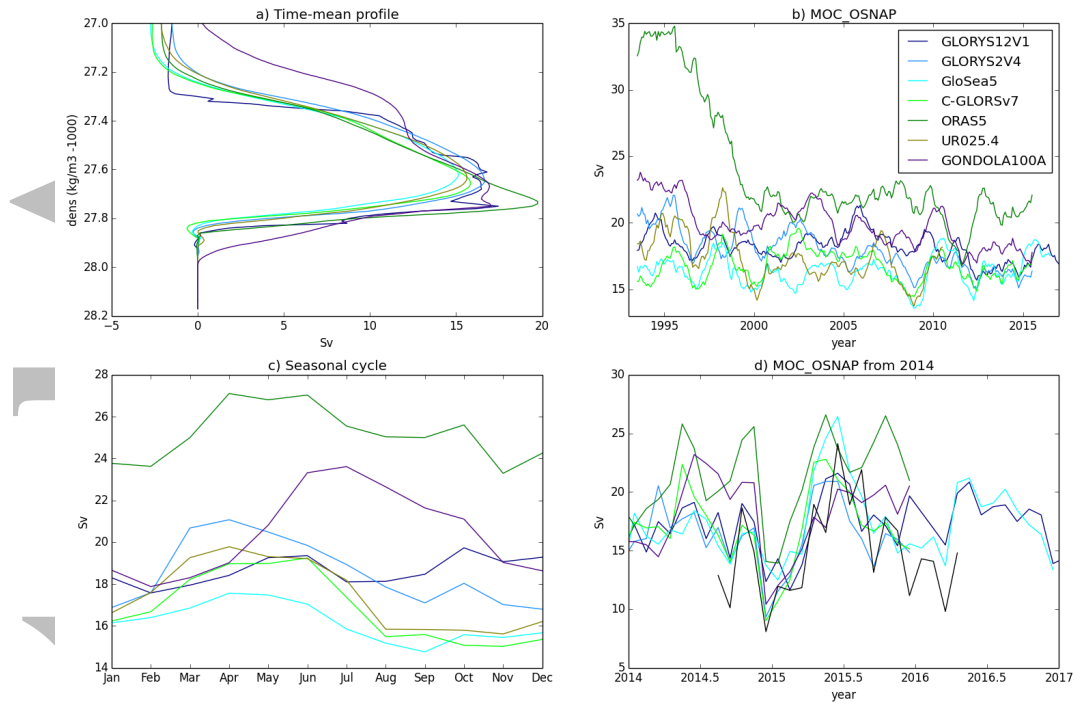


829 **Figure 11.** Timeseries of anomalous AMOC strength (with 12 month running mean). a,c)
 830 Individual models at 26.5°N (thick black line is timeseries from RAPID) and b,d) at 50N. Re-
 831 analyses are split between NEMO and non-NEMO for clarity. e) ensemble mean (black) and
 832 2 x standard deviation (grey) of AMOC anomalies at 26.5°N, with the RAPID anomaly time-
 833 series (thick black). Also shown is the Ekman transport calculated from ERA Interim winds as
 834 in C. D. Roberts et al. (2013a) (blue) f) As e but without observational timeseries and with the
 835 ensemble mean minus Ekman (red). (g,h) Comparisons of AMOC changes across the ensemble.
 836 Each cross is a model, with large crosses assessed as significant changes compared to each model
 837 timeseries. Black crosses are the changes for the ensemble mean and black circles are from the
 838 observations. g) M26 anomaly in 2009.5-2010.5 (compared to 2011-2015 time mean); M26 in
 839 1998.5-1999.5 minus 2000.5-2001.5; M26 in 2005-2007 minus 2000-2002; M26 in 2012-2014 minus
 2005-2007. f) trend in M26 (1993-2016); trend in M50 (1993-2009)



841 **Figure 12.** Taylor diagrams comparing timeseries of observations of AMOC components
 842 from RAPID, with components calculated from the reanalyses using the RAPID methodol-
 843 ogy (C. D. Roberts et al., 2013a). Shown are (a) the AMOC calculated with velocities, (b)
 844 the AMOC and upper ocean components as calculated using the RAPID methodology, (c) the
 845 AMOC and lower ocean components as calculated using the RAPID methodology. Colors show
 846 different reanalyses, symbols show different components. All standard deviations are normal-
 847 ized by the observational standard deviations and all statistics are calculated on annual means.
 848 Note that not all the models have calculated the RAPID decomposition and that models with
 849 insufficient years (UR025.4 and NorCPM-v1) are excluded.

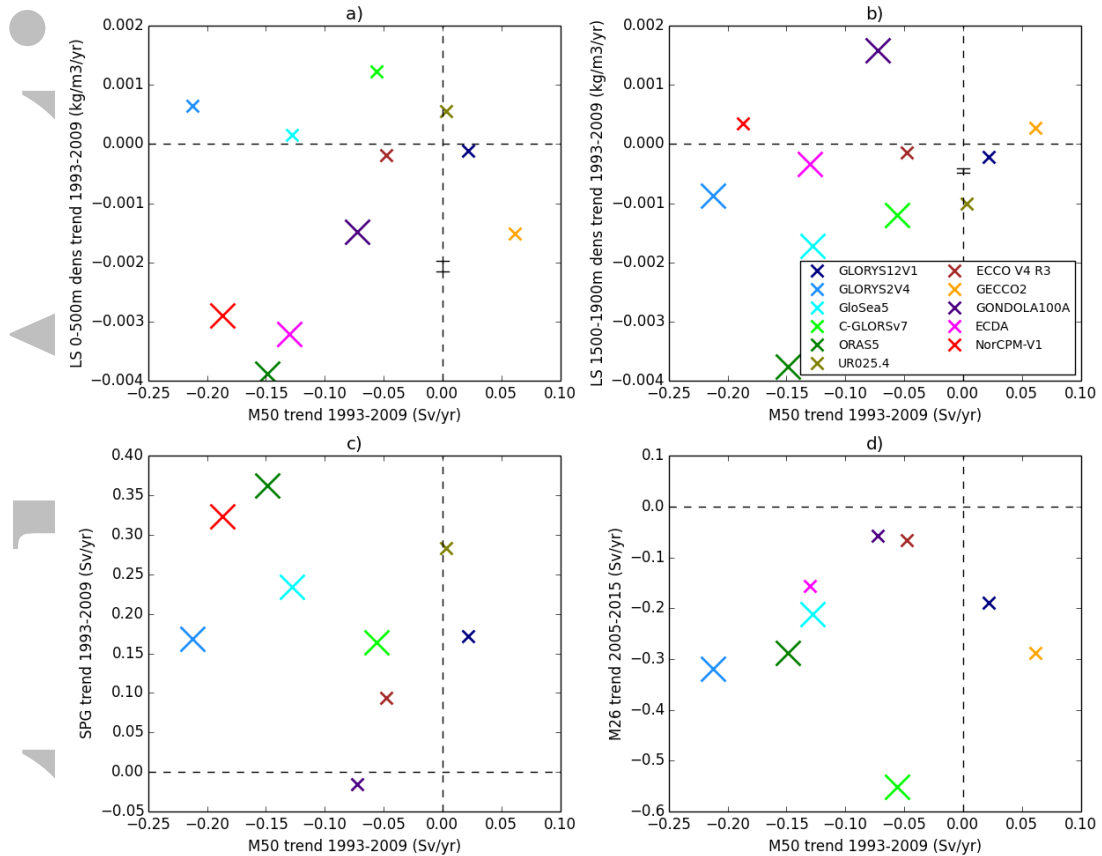
title



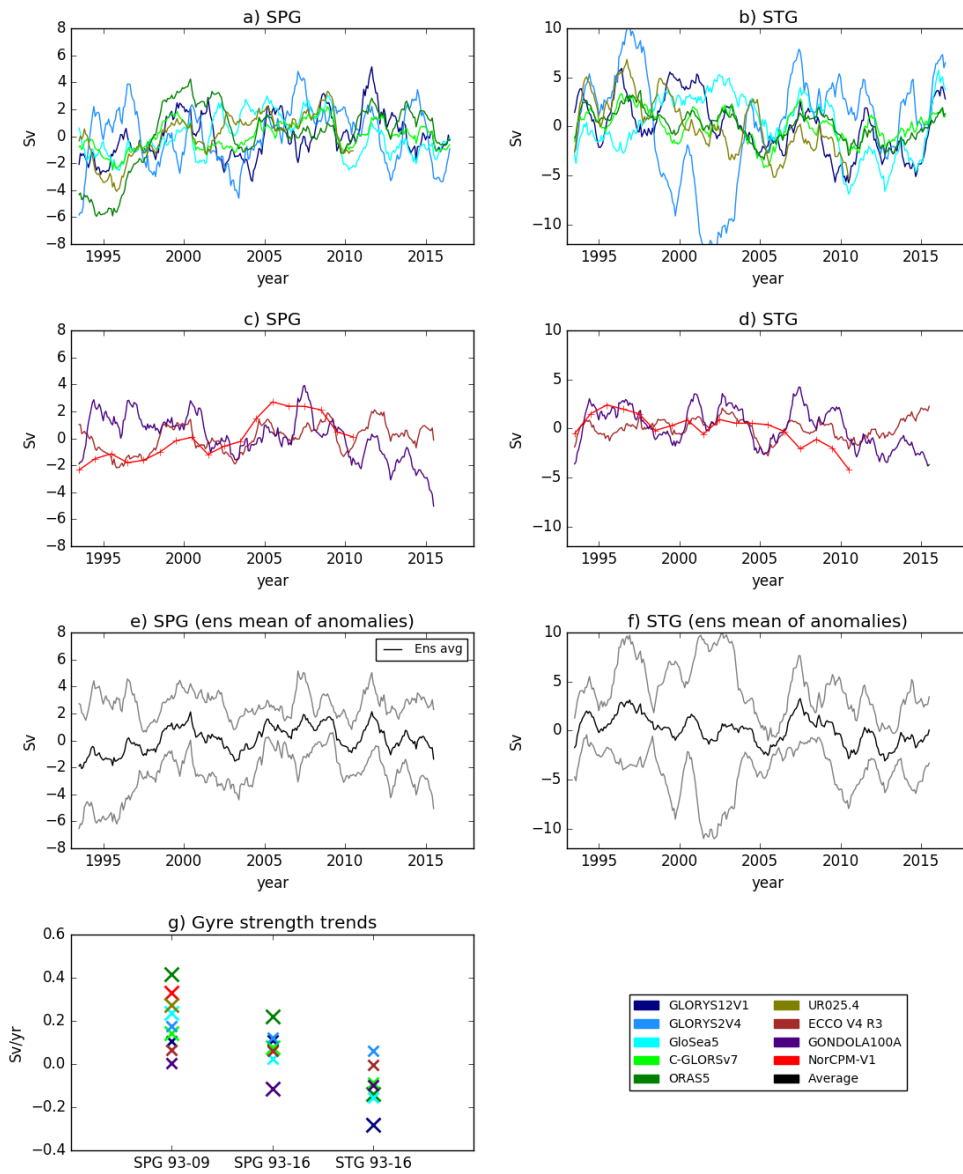
850 **Figure 13.** Overturning in density space along the OSNAP line using potential density ref-
 851 erenced to the surface a) The time mean streamfunction in density space. b) The overturning
 852 strength (maximum in density space) with a 12 month running mean. c) Seasonal cycle of the
 853 overturning strength. d) Monthly values of last few years of overturning strength since 2014. The
 854 black line is the observational estimate from OSNAP (Lozier et al., 2019).

Accepted

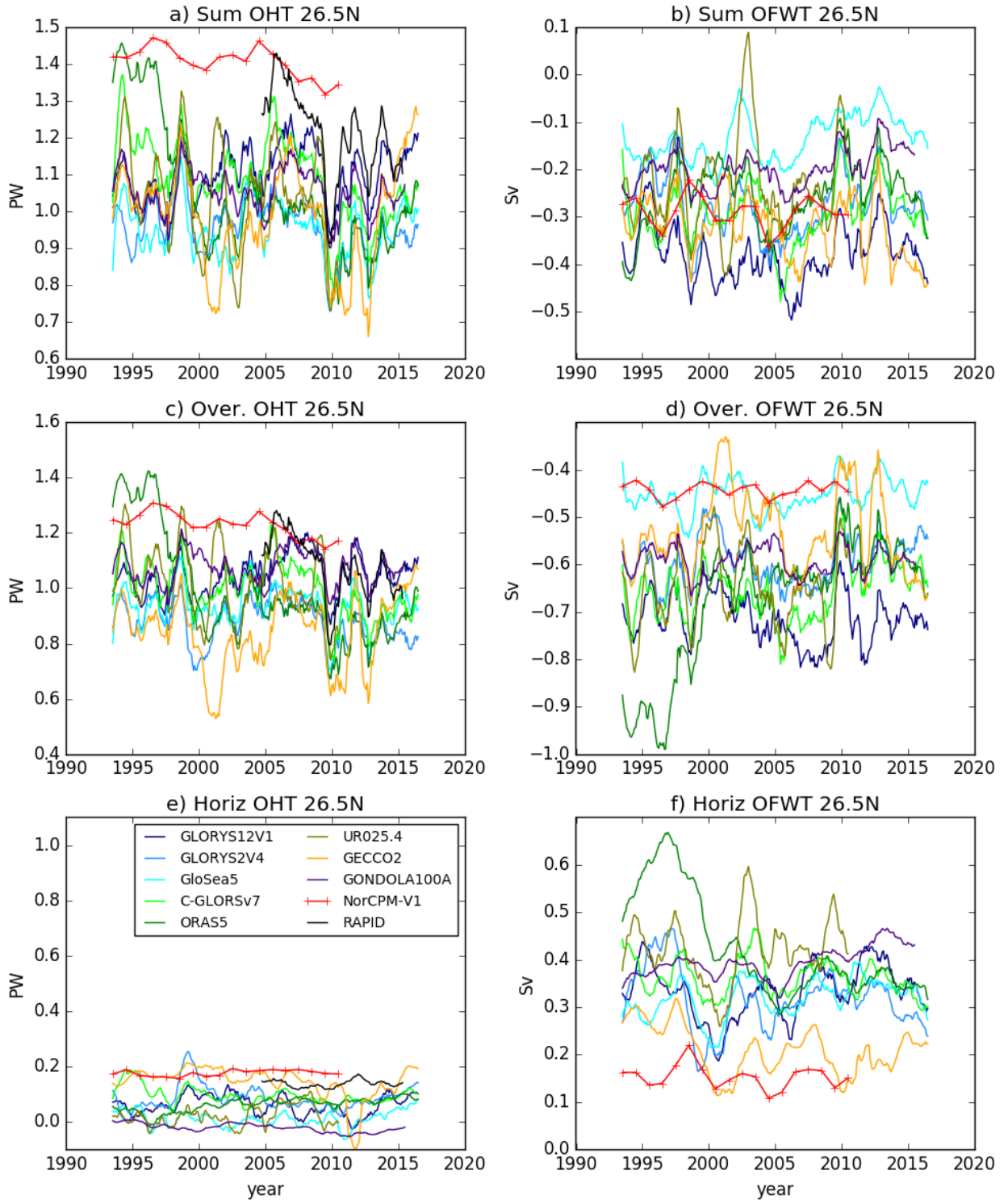
Article



855 **Figure 14.** Comparisons of trends in the Labrador Sea density (0-500m and 1500-1900m),
 856 the SPG and the AMOC 50°N (M50) over the period 1993-2009, and the trend in the AMOC
 857 at 26.5°N (M26) from 2005-2015. All trends are from 1993-2009 apart from M26 which is from
 858 2005-2015. Reanalyses where the trend in both variables is significant (using $p=0.1$) have large
 859 crosses. In panels a and b we also include values of density trends from EN4 and CORA observa-
 860 tional analyses as a black bar. The bar is arbitrarily centered on $x=0$. Dashed lines indicate the
 861 lines of zero trend.



862 **Figure 15.** Timeseries of anomalies of gyre strengths (with 12 month running mean). Note
 863 that GECCO2 has been omitted from this figure because the variability is much larger than
 864 the scales. Individual models for a,c) the SPG (average of the barotropic streamfunction over
 865 60-30°W, 50-60°N) and b,d) the STG (average of the barotropic streamfunction over 80-50°W,25-
 866 38°N). e) ensemble mean (black) and 2 x standard deviation (grey) of SPG timeseries. f) As e
 867 but for the STG. g) Comparisons of trends across the ensemble. Each cross is a model, with large
 868 crosses assessed as significant changes compared to each model timeseries. Black crosses are the
 869 changes for the ensemble mean.



870 **Figure 16.** Heat transports (left hand columns) and freshwater transports (right hand
 871 columns) at 26.5°N. Shown is the gyre component (bottom), the overturning component (middle)
 872 and the sum (top). Note that no throughflow component is included in the sum for the freshwa-
 873 ter transport, making it an equivalent freshwater transport referenced to 26.5°N. For equivalent
 874 freshwater and transport component definitions see McDonagh et al. (2015).

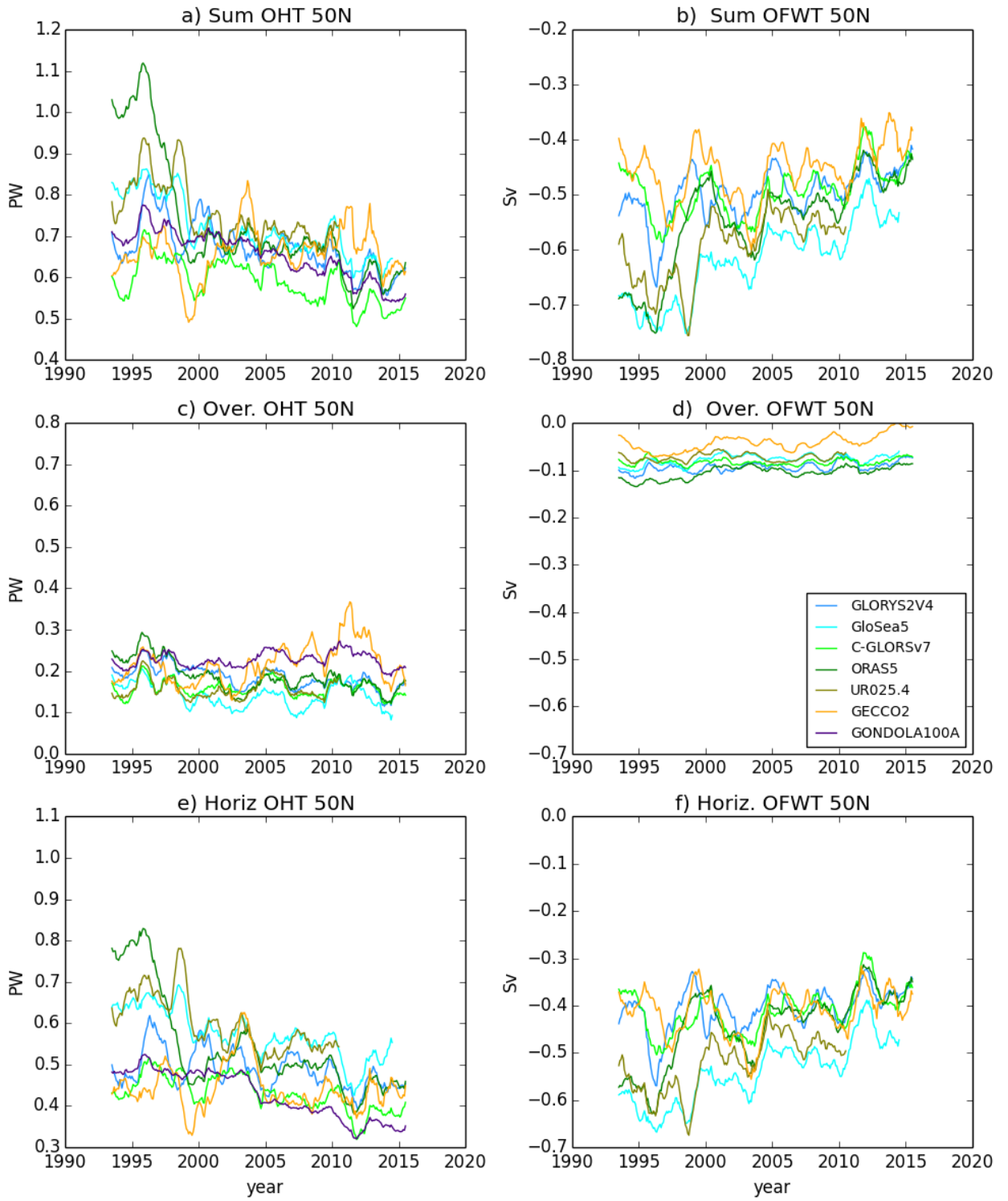
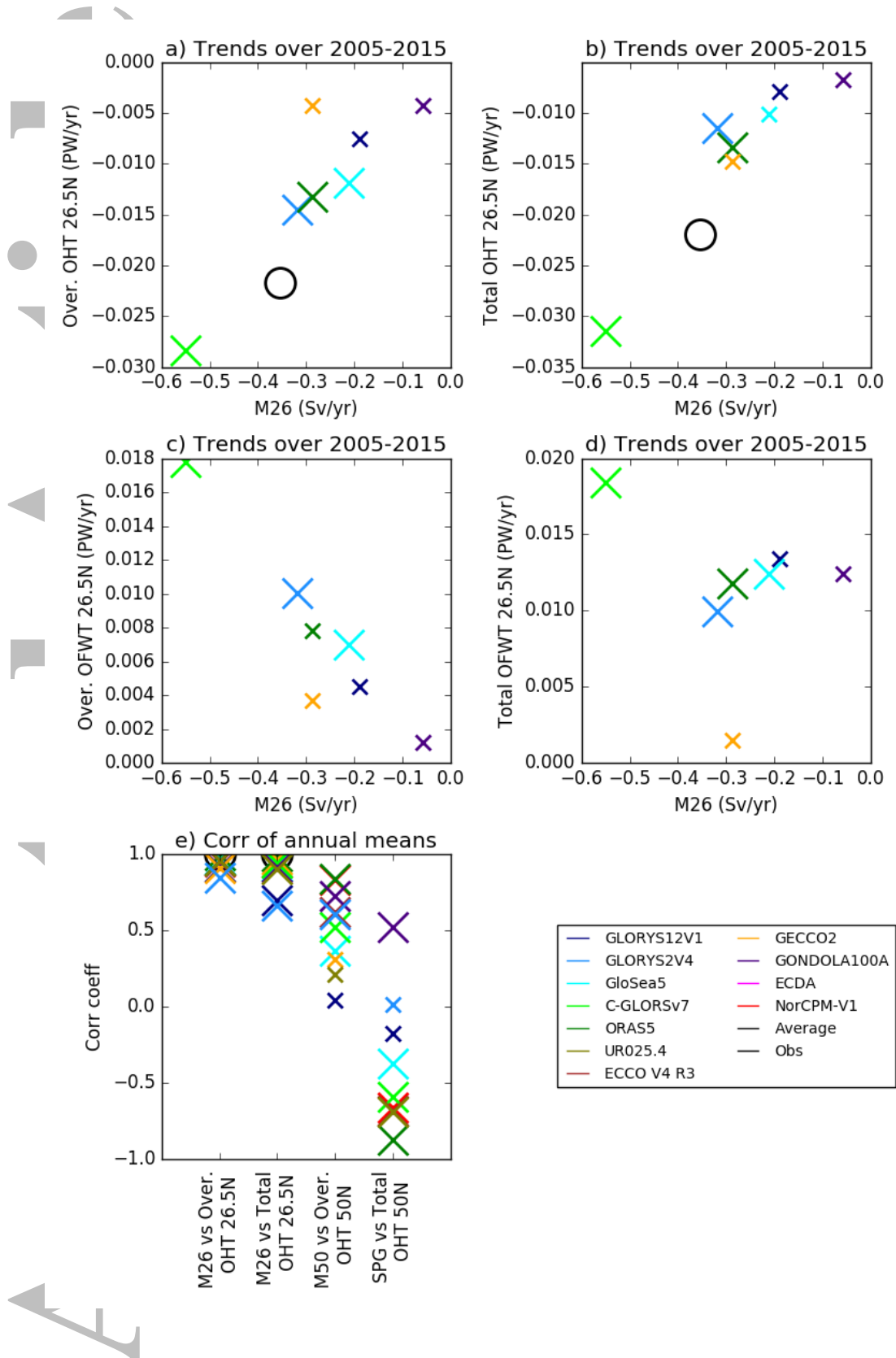


Figure 17. As Fig 16 but at 50°N.



876 **Figure 18.** Comparison of the trends of AMOC at 26.5°N (M26) with trends of a) the over-
 877 turning component of OHT, b) the total heat transport, c) the overturning component of OFWT
 878 d) the total component of OFWT. Trends are over 2005-2015 and those reanalyses where both
 879 variables have significant trends use a large symbol. Observations from RAPID are shown in
 880 black circles. e) Correlations of annual mean time series of M26 and M50 with the overturning
 881 and total components of heat transport. Large crosses show significant relationships.

References

- 909
- 910 Ba, J., Keenlyside, N. S., Latif, M., Park, W., Ding, H., Lohmann, K., ... Volodin,
 911 E. (2014). A multi-model comparison of atlantic multidecadal variability.
 912 *Climate Dynamics*, *43*(9), 2333–2348. doi: 10.1007/s00382-014-2056-1
- 913 Balmaseda, M. A., Hernandez, F., Storto, A., Palmer, M. D., Alves, O., Shi, L.,
 914 ... Gaillard, F. (2015). The Ocean Reanalyses Intercomparison Project
 915 (ORA-IP). *Journal of Operational Oceanography*, *8*(sup1), s80–s97. doi:
 916 10.1080/1755876x.2015.1022329
- 917 Balmaseda, M. A., Smith, G. C., Haines, K., Anderson, D., Palmer, T. N., & Vi-
 918 dard, A. (2007). Historical reconstruction of the Atlantic Meridional Overturn-
 919 ing Circulation from the ECMWF operational ocean reanalysis. *Geophys. Res.*
 920 *Lett.*, *34*(23), L23615+. doi: 10.1029/2007gl031645
- 921 Blockley, E. W., Martin, M. J., McLaren, A. J., Ryan, A. G., Waters, J., Lea, D. J.,
 922 ... Storkey, D. (2014). Recent development of the Met Office operational
 923 ocean forecasting system: an overview and assessment of the new global
 924 FOAM forecasts. *Geoscientific Model Development*, *7*(6), 2613–2638. doi:
 925 10.5194/gmd-7-2613-2014
- 926 Boning, C. W., Scheinert, M., Dengg, J., Biastoch, A., & Funk, A. (2006).
 927 Decadal variability of subpolar gyre transport and its reverberation in
 928 the North Atlantic overturning. *Geophys. Res. Lett.*, *33*, L21S01. doi:
 929 10.1029/2006GL026906
- 930 Bryden, H. L., & Imawaki, I. (2001). Ocean transports of heat. In G. Siedler,
 931 J. Church, & J. Gould (Eds.), *Ocean circulation and climate* (p. 455-474). San
 932 Diego, USA: San Diego Academic Press. doi: 10.1016/S0074-6142(01)80134-0
- 933 Cabanes, C., Grouazel, A., von Schuckmann, K., Hamon, M., Turpin, V.,
 934 Coatanoan, C., ... Le Traon, P. (2013). The CORA dataset: validation and
 935 diagnostics of in-situ ocean temperature and salinity measurements. *Ocean*
 936 *Science*, *9*, 1–18. doi: 10.5194/os-9-1-2013
- 937 Caesar, L., Rahmstorf, S., Robinson, A., Feulner, G., & Saba, V. (2018). Observed
 938 fingerprint of a weakening Atlantic Ocean overturning circulation. *Nature*,
 939 *556*(7700), 191–196. doi: 10.1038/s41586-018-0006-5
- 940 Cassou, C., Deser, C., & Alexander, M. A. (2007). Investigating the impact of
 941 reemerging sea surface temperature anomalies on the winter atmospheric cir-

- 942 culation over the North Atlantic. *Journal of Climate*, 20(14), 3510-3526. doi:
943 10.1175/JCLI4202.1
- 944 Chang, Y., Zhang, S., Rosati, A., Delworth, T., & Stern, W. (2013). An assessment
945 of oceanic variability for 1960-2010 from the GFDL ensemble coupled data
946 assimilation. *Climate Dynamics*, 40, 775-803. doi: 10.1007/s00382-012-1412-2
- 947 Chevallier, M., Smith, G. C., Dupont, F., Lemieux, J.-F., Forget, G., Fujii, Y.,
948 ... Wang, X. (2017). Intercomparison of the arctic sea ice cover in global
949 ocean-sea ice reanalyses from the ora-ip project. *Climate Dynamics*, 49(3),
950 1107-1136. doi: 10.1007/s00382-016-2985-y
- 951 Collins, M., Knutti, R., Arblaster, J., Dufresne, J. L., Fichefet, T., Friedlingstein,
952 P., ... Wehner, M. (2013). Long-term Climate Change: Projections, Com-
953 mitments and Irreversibility. In T. F. Stocker et al. (Eds.), *Climate Change*
954 *2013: The Physical Science Basis. Contribution of Working Group I to the*
955 *Fifth Assessment Report of the Intergovernmental Panel on Climate Change.*
956 Cambridge, United Kingdom and New York, NY, USA.: Cambridge University
957 Press. doi: 10.1017/CBO9781107415324.025
- 958 Counillon, F., Keenlyside, N., Bethke, I., Wang, Y., Billeau, S., Shen, M. L., &
959 Bentsen, M. (2016). Flow-dependent assimilation of sea surface tem-
960 perature in isopycnal coordinates with the Norwegian Climate Prediction
961 Model. *Tellus A: Dynamic Meteorology and Oceanography*, 68(1), 32437. doi:
962 10.3402/tellusa.v68.32437
- 963 Cunningham, S. A., Roberts, C. D., Frajka-Williams, E., Johns, W. E., Hobbs, W.,
964 Palmer, M. D., ... McCarthy, G. (2013). Atlantic Meridional Overturning Cir-
965 culation slowdown cooled the subtropical ocean. *Geophys. Res. Lett.*, 40(23),
966 2013GL058464+. doi: 10.1002/2013gl058464
- 967 Danabasoglu, G., Yeager, S. G., Bailey, D., Behrens, E., Bentsen, M., Bi, D., ...
968 Wang, Q. (2014). North Atlantic simulations in Coordinated Ocean-ice Refer-
969 ence Experiments phase II (CORE-II). Part I: Mean states. *Ocean Modelling*,
970 73, 76 - 107. doi: <https://doi.org/10.1016/j.ocemod.2013.10.005>
- 971 Danabasoglu, G., Yeager, S. G., Kim, W. M., Behrens, E., Bentsen, M., Bi, D., ...
972 Yashayaev, I. (2016). North Atlantic simulations in Coordinated Ocean-ice
973 Reference Experiments phase II (CORE-II). Part II: Inter-annual to decadal
974 variability. *Ocean Modelling*, 97, 65-90. doi: 10.1016/j.ocemod.2015.11.007

- 975 de Boyer-Montegut, C., Madec, G., Fischer, A. S., Lazar, A., & Iudicone, D. (2004).
976 Mixed layer depth over the global ocean: An examination of profile data and a
977 profile-based climatology. *Journal of Geophysical Research: Oceans*, *109*(C12).
978 doi: 10.1029/2004JC002378
- 979 Deshayes, J., & Frankignoul, C. (2008). Simulated variability of the circulation in
980 the North Atlantic from 1953 to 2003. *Journal of Climate*, *21*(19), 4919-4933.
981 doi: 10.1175/2008JCLI1882.1
- 982 Duchez, A., Frajka-Williams, E., Josey, S. A., Evans, D. G., Grist, J. P., Marsh,
983 R., ... Hirschi, J. J.-M. (2016). Drivers of exceptionally cold North Atlantic
984 Ocean temperatures and their link to the 2015 European heat wave. *Environ-*
985 *mental Research Letters*, *11*(7), 074004. doi: 10.1088/1748-9326/11/7/074004
- 986 Dunstone, N., Smith, D., Scaife, A., Hermanson, L., Fereday, D., O'Reilly, C., ...
987 Belcher, S. (2018). Skilful seasonal predictions of summer European rainfall.
988 *Geophysical Research Letters*, *45*(7), 3246-3254. doi: 10.1002/2017GL076337
- 989 Eden, C., & Willebrand, J. (2001). Mechanism of Interannual to Decadal Variabil-
990 ity of the North Atlantic Circulation. *J. Climate*, *14*(10), 2266-2280. doi: 10
991 .1175/1520-0442
- 992 Evans, D. G., Toole, J., Forget, G., Zika, J. D., Naveira Garabato, A. C., Nurser,
993 A. J. G., & Yu, L. (2017). Recent wind-driven variability in Atlantic water
994 mass distribution and meridional overturning circulation. *Journal of Physical*
995 *Oceanography*, *47*(3), 633-647. doi: 10.1175/JPO-D-16-0089.1
- 996 Ferry, N., Parent, L., Garric, G., Bricaud, C., Testut, C.-E., Le Galloudec, O., ...
997 Zawadzki, L. (2012). GLORYS2V1 global ocean reanalysis of the altimetric era
998 (1992-2009) at mesoscale. *Mercator Quarterly Newsletter.*, *44*(44), 29-39.
- 999 Forget, G. (2010). Mapping ocean observations in a dynamical framework: A 2004-
1000 06 ocean atlas. *Journal of Physical Oceanography*, *40*(6), 1201-1221. doi: 10
1001 .1175/2009JPO4043.1
- 1002 Forget, G., Campin, J.-M., Heimbach, P., Hill, C. N., Ponte, R. M., & Wunsch, C.
1003 (2015). ECCO Version 4: an integrated framework for non-linear inverse mod-
1004 eling and global ocean state estimation. *Geoscientific Model Development*, *8*,
1005 3071-3104.
- 1006 Forget, G., & Ponte, R. (2015). The partition of regional sea level variability.
1007 *Progress in Oceanography*, *137*, 173-195.

- 1008 Foukal, N. P., & Lozier, M. S. (2017). Assessing variability in the size and strength
1009 of the North Atlantic subpolar gyre. *Journal of Geophysical Research: Oceans*,
1010 *122*(8), 6295-6308. doi: 10.1002/2017JC012798
- 1011 Fukumori, I., Wang, O., Fenty, I., Forget, G., Heimbach, P., & Ponte, R. M. (2017).
1012 *ECCO Version 4 Release 3* (Tech. Rep.). doi: 1721.1/110380
- 1013 Ganachaud, A., & Wunsch, C. (2003). Large-scale ocean heat and freshwater trans-
1014 ports during the World Ocean Circulation Experiment. *Journal of Climate*,
1015 *16*(4), 696-705. doi: '10.1175/1520-0442(2003)016<0696:LSOHAF>2.0.CO;2'
- 1016 Gent, P. R., & McWilliams, J. C. (1990). Isopycnal mixing in ocean circulation
1017 models. *J. Phys. Oceanogr.*, *20*, 150-155.
- 1018 Good, S. A., Martin, M. J., & Rayner, N. A. (2013). EN4: Quality controlled
1019 ocean temperature and salinity profiles and monthly objective analyses with
1020 uncertainty estimates. *Journal of Geophysical Research*, *118*, 6704-6716.
- 1021 Grist, J., Josey, S., Jacobs, Z., Marsh, R., Sinha, B., & Van Sebille, E. (2016). Ex-
1022 treme air-sea interaction over the North Atlantic subpolar gyre during the
1023 winter of 2013-2014 and its sub-surface legacy. *Climate Dynamics*, *46*(11-12),
1024 4027-4045. doi: 10.1007/s00382-015-2819-3
- 1025 Häkkinen, S., & Rhines, P. B. (2004). Decline of Subpolar North Atlantic Circu-
1026 lation During the 1990s. *Science*, *304*(5670), 555-559. doi: 10.1126/science
1027 .1094917
- 1028 Hatun, H., & Chafik, L. (2018). On the recent ambiguity of the North At-
1029 lantic subpolar gyre index. *Journal of Geophysical Research: Oceans*, *123*,
1030 5072-5076. (<https://doi.org/10.1029/2018JC014101>) doi:
1031 10.1029/2018JC014101
- 1032 Hermanson, L., Eade, R., Robinson, N. H., Dunstone, N. J., Andrews, M. B.,
1033 Knight, J. R., ... Smith, D. M. (2014). Forecast cooling of the Atlantic subpo-
1034 lar gyre and associated impacts. *Geophys. Res. Lett.*, *41*(14), 2014GL060420+.
1035 doi: 10.1002/2014gl060420
- 1036 Heuzé, C. (2017). North Atlantic deep water formation and AMOC in CMIP5 mod-
1037 els. *Ocean Science*, *13*(4), 609-622. doi: 10.5194/os-13-609-2017
- 1038 Jackson, L. C., Peterson, K. A., Roberts, C. D., & Wood, R. A. (2016). Recent slow-
1039 ing of Atlantic overturning circulation as a recovery from earlier strengthening.
1040 *Nature Geosci.*, *9*, 518-522. doi: 10.1038/ngeo2715

- 1041 Johns, W. E., Baringer, M. O., Beal, L. M., Cunningham, S. A., Kanzow, T., Bry-
1042 den, H. L., . . . Curry, R. (2011). Continuous, array-based estimates of Atlantic
1043 Ocean heat transport at 26.5n. *Journal of Climate*, *24*(10), 2429-2449. doi:
1044 10.1175/2010JCLI3997.1
- 1045 Josey, S. A., Hirschi, J. J.-M., Sinha, B., Ducez, A., Grist, J. P., & Marsh, R.
1046 (2018). The recent Atlantic cold anomaly: Causes, consequences, and related
1047 phenomena. *Annual Review of Marine Science*, *10*(1), 475-501. (PMID:
1048 28934597) doi: 10.1146/annurev-marine-121916-063102
- 1049 Karspeck, A. R., Stammer, D., Köhl, A., Danabasoglu, G., Balmaseda, M., Smith,
1050 D. M., . . . Rosati, A. (2017). Comparison of the atlantic meridional over-
1051 turning circulation between 1960 and 2007 in six ocean reanalysis products.
1052 *Climate Dynamics*, *49*(3), 957-982. doi: 10.1007/s00382-015-2787-7
- 1053 Knight, J. R., Allan, R. J., Folland, C. K., Vellinga, M., & Mann, M. E. (2005).
1054 A signature of persistent natural thermohaline circulation cycles in observed
1055 climate. *Geophys. Res. Lett*, *32*. doi: 10.1029/2005GL024233
- 1056 Kohl, A. (2015). Evaluation of the GECCO2 ocean synthesis: transports of volume,
1057 heat and freshwater in the Atlantic. *Quarterly Journal of the Royal Meteorolo-*
1058 *gical Society*, *141*, 166-181.
- 1059 Lellouche, J.-M., Greiner, E., Le Galloudec, O., Garric, G., Regnier, C., Drevillon,
1060 M., . . . Le Traon, P.-Y. (2018). Recent updates to the Copernicus Marine
1061 Service global ocean monitoring and forecasting real-time 1/12 high-resolution
1062 system. *Ocean Science*, *14*, 1093-1126. doi: 10.5194/os-14-1093-2018
- 1063 Lohmann, K., Drange, H., & Bentsen, M. (2009). A possible mechanism for the
1064 strong weakening of the North Atlantic subpolar gyre in the mid-1990s. *Geo-*
1065 *phys. Res. Lett*, *36*, L15602. doi: 10.1029/2009GL039166.
- 1066 Lozier, M. S., Bacon, S., Bower, A. S., Cunningham, S. A., Femke de Jong, M., de
1067 Steur, L., . . . Zika, J. D. (2017). Overturning in the Subpolar North At-
1068 lantic Program: a new international ocean observing system. *Bulletin of the*
1069 *American Meteorological Society*, *98*, 737-752.
- 1070 Lozier, M. S., Li, F., Bacon, S., Bahr, F., Bower, A. S., Cunningham, S. A., . . .
1071 Zhao, J. (2019). A sea change in our view of overturning in the subpolar North
1072 Atlantic. *Science*, *363*(6426), 516-521. doi: 10.1126/science.aau6592
- 1073 Lübbecke, J., Rodriguez-Fonseca, B., Richter, I., Mart in-Rey, M., Losada, T., Polo,

- 1074 I., & Keenlyside, N. (2018). Equatorial Atlantic variability - modes, mecha-
1075 nisms, and global teleconnections. *Wiley Interdisciplinary Reviews: Climate*
1076 *Change*, 9, e527. doi: 10.1002/wcc.527
- 1077 Lumpkin, R., & Speer, K. (2007). Global ocean meridional overturning. *Journal of*
1078 *Physical Oceanography*, 37(10), 2550-2562. doi: 10.1175/JPO3130.1
- 1079 MacLachlan, C., Arribas, A., Peterson, K. A., Maidens, A., Fereday, D., Scaife,
1080 A. A., ... Madec, G. (2015). Global Seasonal forecast system version 5
1081 (GloSea5): a high-resolution seasonal forecast system. *Q. J.R.Meteorol. Soc.*,
1082 141, 1072-1084.
- 1083 Masina, S., Storto, A., Ferry, N., Valdivieso, M., Haines, K., Balmaseda, M., ...
1084 Parent, L. (2017). An ensemble of eddy-permitting global ocean reanaly-
1085 ses from the MyOcean project. *Climate Dynamics*, 49(3), 813-841. doi:
1086 10.1007/s00382-015-2728-5
- 1087 McCarthy, G. D., Frajka-Williams, E., Johns, W. E., Baringer, M. O., Meinen, C. S.,
1088 Bryden, H. L., ... Cunningham, S. A. (2012). Observed interannual variability
1089 of the Atlantic meridional overturning circulation at 26.5N. *Geophys. Res.*
1090 *Lett.*, 39(19), L19609+. doi: 10.1029/2012gl052933
- 1091 McCarthy, G. D., Smeed, D. A., Johns, W. E., Frajka-Williams, E., Moat, B. I.,
1092 Rayner, D., ... Bryden, H. L. (2015). Measuring the Atlantic Meridional
1093 Overturning Circulation at 26N. *Progress in Oceanography*, 130, 91-111. doi:
1094 10.1016/j.pocean.2014.10.006
- 1095 McDonagh, E. L., King, B. A., Bryden, H. L., Courtois, P., Szuts, Z., Baringer,
1096 M., ... McCarthy, G. (2015). Continuous estimate of Atlantic oceanic
1097 freshwater flux at 26.5N. *Journal of Climate*, 28(22), 8888-8906. doi:
1098 10.1175/jcli-d-14-00519.1
- 1099 McDonagh, E. L., McLeod, P., King, B. A., Bryden, H. L., & Valds, S. T. (2010).
1100 Circulation, heat, and freshwater transport at 36n in the Atlantic. *Journal of*
1101 *Physical Oceanography*, 40(12), 2661-2678. doi: 10.1175/2010JPO4176.1
- 1102 Menary, M. B., & Hermanson, L. (2018). Limits on determining the skill of North
1103 Atlantic Ocean decadal predictions. *Nature Communications*, 9(1), 1694-. doi:
1104 10.1038/s41467-018-04043-9
- 1105 Menary, M. B., Hermanson, L., & Dunstone, N. J. (2016). The impact of labrador
1106 sea temperature and salinity variability on density and the subpolar amoc in

- 1107 a decadal prediction system. *Geophys. Res. Lett.*, *43*, 12,217-12,227. doi:
1108 10.1002/2016GL070906
- 1109 Menary, M. B., Hodson, D. L. R., Robson, J. I., Sutton, R. T., Wood, R. A., &
1110 Hunt, J. A. (2015). Exploring the impact of CMIP5 model biases on the sim-
1111 ulation of North Atlantic decadal variability. *Geophysical Research Letters*,
1112 *42*(14), 5926-5934. doi: 10.1002/2015GL064360
- 1113 Mignac, D., Ferreira, D., & Haines, K. (2019). Decoupled freshwater transport
1114 and meridional overturning in the South Atlantic. *Geophysical Research Let-
1115 ters*, *46*. doi: 10.1029/2018GL081328
- 1116 Msadek, R., Johns, W. E., Yeager, S. G., Danabasoglu, G., Delworth, T. L., &
1117 Rosati, A. (2013). The Atlantic Meridional Heat Transport at 26.5N
1118 and Its Relationship with the MOC in the RAPID Array and the GFDL
1119 and NCAR Coupled Models. *Journal of Climate*, *26*(12), 4335-4356. doi:
1120 10.1175/JCLI-D-12-00081.1
- 1121 Palmer, M. D., & Haines, K. (2009). Estimating oceanic heat content change using
1122 isotherms. *Journal of Climate*, *22*(19), 4953-4969. doi: 10.1175/2009JCLI2823
1123 .1
- 1124 Palmer, M. D., Roberts, C. D., Balmaseda, M., Chang, Y.-S., Chepurin, G., Ferry,
1125 N., ... Xue, Y. (2017). Ocean heat content variability and change in an
1126 ensemble of ocean reanalyses. *Climate Dynamics*, *49*(3), 909-930. doi:
1127 10.1007/s00382-015-2801-0
- 1128 Peings, Y., & Magnusdottir, G. (2014). Forcing of the wintertime atmospheric circu-
1129 lation by the multidecadal fluctuations of the North Atlantic ocean. *Environ-
1130 mental Research Letters*, *9*(3), 034018+. doi: 10.1088/1748-9326/9/3/034018
- 1131 Piecuch, C. G., Ponte, R. M., Little, C. M., Buckley, M. W., & Fukumori, I.
1132 (2017). Mechanisms underlying recent decadal changes in subpolar North
1133 Atlantic Ocean heat content. *J. Geophys. Res. Oceans*, *122*, 7181-7197. doi:
1134 10.1002/2017JC012845
- 1135 Rhein, M., Rintoul, S., Aoki, S., Campos, E., Chambers, D., Feely, R., ... Wang,
1136 F. (2013). Observations: Ocean. In T. Stocker et al. (Eds.), *Climate Change
1137 2013: The Physical Science Basis. Contribution of Working Group I to the
1138 Fifth Assessment Report of the Intergovernmental Panel on Climate Change*
1139 (p. 255-316). Cambridge, United Kingdom and New York, NY, USA: Cam-

- 1140 bridge University Press. doi: 10.1017/CBO9781107415324.010
- 1141 Roberts, C. D., Garry, F. K., & Jackson, L. C. (2013b). A Multimodel Study of
1142 Sea Surface Temperature and Subsurface Density Fingerprints of the Atlantic
1143 Meridional Overturning Circulation. *J. Climate*, *26*(22), 9155–9174. doi:
1144 10.1175/jcli-d-12-00762.1
- 1145 Roberts, C. D., Waters, J., Peterson, K. A., Palmer, M. D., McCarthy, G. D.,
1146 Frajka-Williams, E., ... Zuo, H. (2013a). Atmosphere drives recent inter-
1147 annual variability of the Atlantic meridional overturning circulation at 26.5N.
1148 *Geophys. Res. Lett.*, *40*(19), 5164–5170. doi: 10.1002/grl.50930
- 1149 Roberts, M. J., Hewitt, H. T., Hyder, P., Ferreira, D., Josey, S. A., Mizielinski, M.,
1150 & Shelly, A. (2016). Impact of ocean resolution on coupled air-sea fluxes and
1151 largescale climate. *Geophysical Research Letters*, *43*, 10,430–10,438.
- 1152 Robson, J., Hodson, D., Hawkins, E., & Sutton, R. (2014). Atlantic overturning in
1153 decline? *Nature Geoscience*, *7*(1), 2–3. doi: 10.1038/ngeo2050
- 1154 Robson, J., Ortega, P., & Sutton, R. (2016). A reversal of climatic trends in the
1155 North Atlantic since 2005. *Nature Geoscience*, *9*(7), 513–517. doi: 10.1038/
1156 ngeo2727
- 1157 Robson, J., Sutton, R., Lohmann, K., Smith, D., & Palmer, M. D. (2012). Causes of
1158 the Rapid Warming of the North Atlantic Ocean in the Mid-1990s. *J. Climate*,
1159 *25*(12), 4116–4134. doi: 10.1175/jcli-d-11-00443.1
- 1160 Robson, J., Sutton, R. T., Archibald, A., & et al. (2018). Recent multivariate
1161 changes in the North Atlantic climate system, with a focus on 2005- 2016. *Int*
1162 *J Climatol*, *38*, 5050-5076. doi: 10.1002/joc.5815
- 1163 Shi, L., Alves, O., Wedd, R., Balmaseda, M. A., Chang, Y., Chepurin, G., ... Yin,
1164 Y. (2017). "an assessment of upper ocean salinity content from the ocean
1165 reanalyses inter-comparison project (ora-ip)". *Climate Dynamics*, *49*(3),
1166 1009–1029. doi: 10.1007/s00382-015-2868-7
- 1167 Smeed, D. A., Josey, S. A., Beaulieu, C., Johns, W. E., Moat, B. I., Frajka-Williams,
1168 E., ... McCarthy, G. D. (2018). The North Atlantic Ocean Is in a State
1169 of Reduced Overturning. *Geophys. Res. Lett.*, *45*, 2017GL076350+. doi:
1170 10.1002/2017gl076350
- 1171 Smeed, D. A., McCarthy, G., Rayner, D., Moat, B., Johns, W., Baringer, M., &
1172 Meinen, C. (2017). *Atlantic meridional overturning circulation observed by*

- 1173 the RAPID-MOCHA-WBTS (*RAPID-Meridional Overturning Circulation and*
 1174 *Heatflux Array-Western Boundary Time Series*) array at 26N from 2004 to
 1175 2017. Natural Environment Research Council, UK.: British Oceanographic
 1176 Data Centre. Retrieved from [https://www.rapid.ac.uk/rapidmoc/rapid](https://www.rapid.ac.uk/rapidmoc/rapid_data/datadl.php)
 1177 [_data/datadl.php](https://www.rapid.ac.uk/rapidmoc/rapid_data/datadl.php) doi: 10.5285/5acfd143-1104-7b58-e053-6c86abc0d94b
- 1178 Smith, D., Eade, R., Dunstone, N., Fereday, D., Murphy, J., Pohlman, H., & Scaife,
 1179 A. (2010). Skillful multi-year predictions of Atlantic hurricane frequency.
 1180 *Nature Geoscience*, 3, 846-849. doi: doi:10.1038/NGEO1004
- 1181 Stepanov, V. N., Iovino, D., Masina, S., Storto, A., & Cipollone, A. (2016).
 1182 Observed and simulated variability of the Atlantic Meridional Overturn-
 1183 ing Circulation at 41N. *Journal of Marine Systems*, 164, 42–52. doi:
 1184 10.1016/j.jmarsys.2016.08.004
- 1185 Storto, A., Alvera-Azcarate, A., Balmesada, M. A., Barth, A., Chevallier, M.,
 1186 Counillon, F., ... Zuo, H. (2019). Ocean reanalyses: recent advances and
 1187 unsolved challenges. *Frontiers in Marine Science*, 6, 418.
- 1188 Storto, A., & Masina, S. (2016). C-GLORSv5: an improved multipurpose global
 1189 ocean eddy-permitting physical reanalysis. *Earth Syst. Sci. Data*, 8, 679-696.
 1190 doi: 10.5194/essd-8-679-2016
- 1191 Storto, A., Masina, S., Balmaseda, M., Guinehut, S., Xue, Y., Szekely, T., ... Wang,
 1192 X. (2017). Steric sea level variability (1993–2010) in an ensemble of ocean
 1193 reanalyses and objective analyses. *Climate Dynamics*, 49(3), 709–729. doi:
 1194 10.1007/s00382-015-2554-9
- 1195 Storto, A., Masina, S., & Navarra, A. (2016). Evaluation of the CMCC eddy-
 1196 permitting global ocean physical reanalysis system (C-GLORS, 1982-2012)
 1197 and its assimilation components. *Q.J.R. Meteorol. Soc.*, 142, 738-758. doi:
 1198 10.1002/qj.2673
- 1199 Storto, A., Masina, S., Simoncelli, S., Iovino, D., Cipollone, A., Drevillon, M.,
 1200 ... Peterson, K. A. (2018). The added value of the multi-system spread
 1201 information for ocean heat content and steric sea level investigations in
 1202 the cmems grep ensemble reanalysis product. *Climate Dynamics*. doi:
 1203 10.1007/s00382-018-4585-5
- 1204 Sutton, R. T., & Dong, B. (2012). Atlantic Ocean influence on a shift in European
 1205 climate in the 1990s. *Nature Geosci*, 5(11), 788–792. doi: 10.1038/ngeo1595

- 1206 Sutton, R. T., McCarthy, G. D., Robson, J., Sinha, B., Archibald, A. T., & Gray,
1207 L. J. (2018). Atlantic multidecadal variability and the u.k. acsis pro-
1208 gram. *Bulletin of the American Meteorological Society*, *99*(2), 415-425. doi:
1209 10.1175/BAMS-D-16-0266.1
- 1210 Talley, L. D. (2003). Shallow, intermediate, and deep overturning components of the
1211 global heat budget. *Journal of Physical Oceanography*, *33*(3), 530-560. doi:
1212 {10.1175/1520-0485(2003)033<0530:SIADOC>2.0.CO;2}
- 1213 Talley, L. D. (2008). Freshwater transport estimates and the global overturning cir-
1214 culation: Shallow, deep and throughflow components. *Progress in Oceanogra-*
1215 *phy*, *78*(4), 257 - 303. doi: 10.1016/j.pocean.2008.05.001
- 1216 Tett, S. F. B., Sherwin, T. J., Shrivastava, A., & Browne, O. (2014). How Much Has the
1217 North Atlantic Ocean Overturning Circulation Changed in the Last 50 Years?
1218 *J. Climate*, *27*(16), 6325–6342. doi: 10.1175/jcli-d-12-00095.1
- 1219 Thornalley, D. J. R., Oppo, D. W., Ortega, P., Robson, J. I., Brierley, C. M., Davis,
1220 R., ... Keigwin, L. D. (2018). Anomalously weak Labrador Sea convection and
1221 Atlantic overturning during the past 150 years. *Nature*, *556*(7700), 227–230.
1222 doi: 10.1038/s41586-018-0007-4
- 1223 Tietsche, S., Balmaseda, M. A., Zuo, H., & Mogensen, K. (2017). Arctic sea ice in
1224 the global eddy-permitting ocean reanalysis orap5. *Climate Dynamics*, *49*(3),
1225 775–789. doi: 10.1007/s00382-015-2673-3
- 1226 Toyoda, T., Fujii, Y., Kuragano, T., Kamachi, M., Ishikawa, Y., Masuda, S., ...
1227 Lee, T. (2017a). Intercomparison and validation of the mixed layer depth
1228 fields of global ocean syntheses. *Climate Dynamics*, *49*(3), 753–773. doi:
1229 10.1007/s00382-015-2637-7
- 1230 Toyoda, T., Fujii, Y., Kuragano, T., Kosugi, N., Sasano, D., Kamachi, M., ... Bal-
1231 maseda, M. (2017b). Interannual-decadal variability of wintertime mixed
1232 layer depths in the north pacific detected by an ensemble of ocean syntheses.
1233 *Climate Dynamics*, *49*(3), 891–907. doi: 10.1007/s00382-015-2762-3
- 1234 Toyoda, T., Fujii, Y., Yasuda, T., Usui, N., Ogawa, K., Kuragano, T., ... Kamachi,
1235 M. (2016). Data assimilation of sea ice concentration into a global ocean-sea
1236 ice model with corrections for atmospheric forcing and ocean temperature
1237 fields. *J Oceanogr*, *72*, 235-262. doi: 10.1007/s10872-015-0326-0
- 1238 Treguier, A. M., Deshayes, J., Lique, C., Dussin, R., & Molines, J. M. (2012). Eddy

- 1239 contributions to the meridional transport of salt in the North Atlantic. *Journal*
1240 *of Geophysical Research: Oceans*, *117*, C05010. doi: 10.1029/2012JC007927
- 1241 Uotila, P., Goosse, H., Haines, K., Chevallier, M., Barthélemy, A., Bricaud, C., ...
1242 Zhang, Z. (2018). An assessment of ten ocean reanalyses in the polar regions.
1243 *Climate Dynamics*. doi: 10.1007/s00382-018-4242-z
- 1244 Vage, K., Pickart, R. S., Thierry, V., Reverdin, G., Lee, C. M., Petrie, B., ... Riber-
1245 gaard, M. H. (2008). Surprising return of deep convection to the subpolar
1246 North Atlantic Ocean in winter 2007-2008. *Nature Geoscience*, *2*, 67-.
- 1247 Valdivieso, M., Haines, K., Balmaseda, M., Chang, Y.-S., Drevillon, M., Ferry, N.,
1248 ... Andrew Peterson, K. (2017). An assessment of air-sea heat fluxes from
1249 ocean and coupled reanalyses. *Climate Dynamics*, *49*(3), 983-1008. doi:
1250 10.1007/s00382-015-2843-3
- 1251 Valdivieso, M., Haines, K., Zuo, H., & Lea, D. (2014). Freshwater and heat trans-
1252 ports from global ocean synthesis. *J. Geophys. Res. Oceans*, *119*(1), 394-409.
1253 doi: 10.1002/2013jc009357
- 1254 von Schuckmann, K., & et al. (2018). Copernicus Marine Service Ocean State Re-
1255 port 2. *Journal of Operational Oceanography*, *11:sup1*, S1-S142. doi: 10.1080/
1256 1755876X.2018.1489208
- 1257 Wang, Y., Counillon, F., Bethke, I., Keenlyside, N., Bocquet, M., & Shen, M.
1258 (2017). Optimising assimilation of hydrographic profiles into isopycnal ocean
1259 models with ensemble data assimilation. *Ocean Modelling*, *114*, 3344. doi:
1260 10.1016/j.ocemod.2017.04.007
- 1261 Wijffels, S. E. (2001). Ocean transport of fresh water. In G. Siedler, J. Church, &
1262 J. Gould (Eds.), *Ocean circulation and climate* (p. 475-488). San Diego, USA:
1263 San Diego Academic Press. doi: 10.1016/S0074-6142(01)80135-2
- 1264 Williams, R. G., Roussenov, V., Smith, D., & Lozier, M. S. (2014). Decadal Evo-
1265 lution of Ocean Thermal Anomalies in the North Atlantic: The Effects of
1266 Ekman, Overturning, and Horizontal Transport. *Journal of Climate*, *27*(2),
1267 698-719. doi: 10.1175/JCLI-D-12-00234.1
- 1268 Yang, C., Masina, S., Bellucci, A., & Storto, A. (2016). The Rapid Warming of the
1269 North Atlantic Ocean in the Mid-1990s in an Eddy-Permitting Ocean Reanaly-
1270 sis (1982-2013). *J. Climate*, *29*(15), 5417-5430. doi: 10.1175/jcli-d-15-0438.1
- 1271 Yashayaev, I., & Loder, J. W. (2017). Further intensification of deep convection in

- 1272 the Labrador Sea in 2016. *Geophys. Res. Lett.*, *44*(3), 2016GL071668+. doi: 10
1273 .1002/2016gl071668
- 1274 Yeager, S. (2015). Topographic coupling of the Atlantic overturning and gyre circu-
1275 lations. *Journal of Physical Oceanography*, *45*(5), 1258-1284. doi: 10.1175/JPO
1276 -D-14-0100.1
- 1277 Yeager, S., & Danabasoglu, G. (2014). The Origins of Late-Twentieth-Century Vari-
1278 ations in the Large-Scale North Atlantic Circulation. *J. Climate*, *27*(9), 3222-
1279 3247. doi: 10.1175/jcli-d-13-00125.1
- 1280 Zhang, R., & Delworth, T. L. (2006). Impact of Atlantic multidecadal oscillations on
1281 India/Sahel rainfall and Atlantic hurricanes. *Geophys. Res. Lett.*, *33*, L17712.
1282 doi: 10.1029/2006GL026267.
- 1283 Zhang, S., Harrison, M. J., Rosati, A., & Wittenberg, A. T. (2007). System design
1284 and evaluation of coupled ensemble data assimilation for global oceanic climate
1285 studies. *Monthly Weather Review*, *135*, 3541-3564. doi: 10.1175/MWR3466.1
- 1286 Zuo, H., A, B. M., Tietsche, S., Mogensen, K., & Mayer, M. (2019). The ECMWF
1287 operational ensemble reanalysis-analysis system for ocean and sea-ice: a
1288 description of the system and assessment. *Ocean Sci.*, *15*, 779-808. doi:
1289 10.5194/os-15-779-2019